Proteostasis failure and mitochondrial dysfunction contribute to chromosomal instability-induced microcephaly

Amanda González-Blanco[1], Adrián Acuña-Higaki[1], David Boettger[1], Jery Joy[1,2], and Marco Milán[1,3 *]

[1]Institute for Research in Biomedicine (IRB Barcelona), The Barcelona Institute of Science and Technology, Baldiri Reixac, 10, 08028 Barcelona, Spain.

[2] Present address: Bakar Aging Research Institute

University of California, San Francisco, CA 94143, USA

[3]Institució Catalana de Recerca i Estudis Avançats (ICREA)

Pg. Lluís Companys 23, 08010 Barcelona, Spain

[*] email: marco.milan@irbbarcelona.org

Abstract

Mosaic variegated aneuploidy (MVA), a rare human congenital disorder that causes microcephaly, is characterized by extensive abnormalities in chromosome number and results from mutations in genes involved in accurate mitotic chromosome segregation. To characterize the cellular mechanisms underlying this disease, here we generated a *Drosophila* model of microcephaly caused by the depletion of a single spindle assembly checkpoint (SAC) gene in the neural stem cell (NSC) compartment. We present evidence that loss of stemness - compromised identity and proliferative capacity of NSCs- plays an important role in MVA and results in a reduced number of neurons and glial cells. We show that loss of stemness arises from the accumulation over time of an unbalanced number of gains and losses of more than one chromosome, rather than a direct consequence of chromosomal instability-induced DNA damage or the production of simple aneuploidies. We unravel a contribution of proteostasis failure and mitochondrial dysfunction to the negative impact of complex aneuploidies on stemness, a highly energy demanding cellular state. We identify overexpression of Radical Oxygen Species scavengers, mitochondria chaperones and apoptosis inhibition as genetic interventions capable of dampening the deleterious effects of aneuploidy on brain size.

Introduction

Mosaic variegated aneuploidy (MVA) is characterized by widespread mosaic aneuploidies, involving different chromosomes and tissues. MVA patients can present growth retardation, early childhood cancer, and microcephaly [1–4]. MVA is caused by pathogenic mutations in components of the spindle-assembly checkpoint (SAC) and proteins involved in centrosome dynamics during mitosis [5–10]. In cells from MVA patients carrying bi-allelic mutations in these genes, defects in chromosome segregation cause chromosomal instability (CIN), which results in the generation of aneuploid karyotypes. In mouse models of MVA-driven microcephaly caused by mutations in SAC genes, a dramatic reduction in the neural stem cells (NSCs), their intermediate progenitors, and post-mitotic neurons is associated with massive cell death [11], which is largely independent of the tumor suppressor gene p53 [12]. The *Drosophila* brain, whose development and growth also relies on the proliferative activity of NSCs, has proven to be a valuable model in which to demonstrate a causal relationship between chromosome segregation errors and microcephaly [13–15]. By combining changes in centrosome number (amplification or loss) with mutations in SAC genes or by acute targeting of chromosome cohesion, these studies have shown that the resulting brains present extensive abnormalities in chromosome number, a dramatic reduction of the NSC population, and small brain size. Unfortunately, the underlying cellular and molecular mechanisms leading to NSC loss and microcephaly are largely unidentified.

Here we have generated a fly model of microcephaly caused by depletion of a single SAC gene, as occurs in MVA patients. We present evidence that targeted depletion of the SAC in NSCs induces microcephaly in flies and that loss of NSC stemness—compromised identity and proliferative capacity—plays an important role of the disease and results in a reduced number of neurons and glial cells. We have characterized the response of the developing brain to CIN-induced DNA damage and different types and levels of aneuploidy and have identified the cellular and molecular mechanisms causing CIN-induced loss of NSC stemness. We present evidence that NSCs are highly resistant to DNA damage and that simple aneuploidies, consisting of single chromosome gains, have a mild impact on the identity and proliferative capacity of these cells and on brain size. In contrast,

our results indicate that loss of stemness of SAC-depleted NSCs results from the accumulation, through consecutive cell cycles, of complex aneuploidies consisting of an unbalanced number of gains and losses of more than one chromosome. We performed transcriptomic analysis to unveil a strong effect of CIN on cellular homeostasis. Thus, SAC-depleted brains showed a reduction in genes involved in ribosome biogenesis and RNA metabolism, activation of protein quality control mechanisms (autophagy), and reduction in mitochondrial activity. We demonstrate that proteostasis failure—most probably due to aneuploidy-induced gene dosage and proteome imbalance—and mitochondrial dysfunction contribute to the deleterious effects of complex aneuploidies on NSC stemness, a highly energy demanding cellular state. Lastly, we present evidence that genetic interventions aimed at restoring mitochondrial homeostasis and blocking apoptosis can mitigate the negative impact of complex aneuploidies on brain size.

Results

Targeted depletion of SAC genes in neural stem cells induces microcephaly

The central region of the *Drosophila* larval brain contains neural stem cells (NSCs), which are of embryonic origin and re-enter the cell cycle after a quiescence period in the first instar larval stage (around 32 hours after egg laying, AEL) [16]. Among them, we find the type I neuroblasts (NBs), which divide asymmetrically to self-renew and produce ganglion mother cells (GMCs), which will divide once more to give rise to two neurons or glial cells. NBs will differentiate into GMCs or die at the end of larval development, and differentiating neurons and glial cells will build the adult central brain (Fig. 1D). In humans, MVA-driven microcephaly is caused in half of the patients by bi-allelic mutations in single genes with well-documented roles in spindle assembly checkpoint (SAC) function or correct kinetochore-microtubule attachment [5–10]. Our first aim was then to address whether targeted depletion of a single SAC gene could also cause a reduction in larval brain size in flies and whether NBs were the most susceptible cells to CIN. We used the *worniu-gal4* driver to induce chronic expression of RNAi forms against the SAC genes *bub3* or *rod* specifically in NBs and to analyze the total number of NBs (labeled by a nuclear GFP/ß-galactosidase fusion protein expressed by the *UAS-GFP-nuc-lacZ* transgene [17] and by expression of Deadpan, Dpn), GMCs (labeled by the expression

of Prospero, Pros), neurons (labeled by the expression of Elav), and glial cells (labeled by the expression of Repo), as well as the size of the brain lobe. We analyzed control brains and brains subjected to chronic SAC depletion in proliferating NBs at four time points of larval development (in second instar at 48 and 62 h AEL, and in third instar at 72 and 96 h AEL). In control flies not subjected to SAC depletion, NB number in the central brain remained constant throughout larval development, and the number of Pros+ cells and the size of the resulting brain increased as a result of the active proliferative capacity of NBs (Fig. 1A, A'). In contrast, in flies subjected to chronic SAC depletion, the number of NBs was gradually reduced (Fig. 1A, A') and this reduction was highest at later stages of development (Fig. 1A, A' and Supplementary Fig.1A, A'). We noticed that developmental timing was not affected by SAC depletion (Supplementary Fig. 1C), and that the expression levels of the Bub3 protein were already compromised at early stages (48 h AEL, Supplementary Fig. 1D). The gradual decrease in the number of NBs was also observed upon temporally controlled depletion of the SAC gene using the thermo-sensitive Gal80 system (Supplementary Fig. 1E, E'). In this experimental setup, expression of *bub3-RNAi* was restricted to the last 24, 48 or 72 hours of development and NB number was quantified at 96 h AEL. Remarkably, at least 48 h of *bub3* depletion were required to get a significant effect on NB number (Supplementary Fig. 1E, E'), despite the rapid cell cycles of this population (every 2 h) at these developmental stages [18]. We also noticed that activity of the SAC was already compromised after 24h of RNAi expression (Supplementary Fig. 1F). These results point to a delayed response of NBs to CIN, as previously shown [14]. Consistent with this delayed response, only a significant reduction in the number of Pros+ cells and in brain size was observed at later stages of larval development upon chronic depletion of the SAC (Fig. 1A, A', see also Supplementary Fig. 1A'). The size of the brain of those adults that survived to chronic depletion of the SAC was also significantly reduced (Fig. 1E). As expected, the number of neurons and glial cells in developing SAC-depleted brains was also reduced when compared to control brains (Fig. 1B, B', see also Supplementary Fig. 1A'). These results indicate that the impact of SAC depletion on brain size is a result of a reduced number of GMCs, neurons, and glial cells. To reinforce this notion, we performed lineage tracing of the progeny of control and SAC-depleted NBs using the G-TRACE technique [19]. As

shown in Fig. 1C, C', the area covered by the progeny of SAC-depleted NBs was reduced when compared to control samples.

Targeted depletion of SAC genes induces cell cycle arrest in NSCs

We noticed in control brains expressing the *UAS-GFP-nuc-lacZ* transgene under the control of the *worniu-gal4* driver that the GFP protein was not restricted to NBs and was inherited through perdurance of the Gal4 or GFP proteins by their daughter cells, the GMCs (Fig. 1A, lower panels). In contrast, in brains subjected to SAC depletion, the expression of this transgene was very often restricted to NBs and was not observed in the surrounding GMCs, thereby pointing to a failure in the proliferative activity of NBs upon prolonged SAC depletion (see also [13]). Mitotic activity, monitored with an antibody against a phosphorylated form of histone H3 at serine 10 (PH3) that labels mitotic figures, was first quantified in control and SAC-depleted NBs. As shown in Fig. 2A, A', mitotic activity was compromised in SAC-depleted NBs of mature larval brains. This reduction in mitotic activity was already visible at early larval stages (Fig. 2B, B'). We also monitored S phase progression by exposing larval brains to 5-ethynyl-2′-deoxyuridine (EdU) for 45 min and subsequently analyzing its incorporation. The number of EdU-positive NBs was also reduced in SAC-depleted brains when compared to control samples (Fig. 2A, A'). Using Fly-Fucci, which relies on fluorochrome-tagged degrons from the Cyclin B (in red) and E2F1 (in green) proteins which are degraded during mitosis or at the onset of the S phase, respectively [20] , we observed that the number of cells not expressing either of these markers and potentially arrested in late G1 were largely increased in SAC-depleted NBs (Fig. 2C, C'). A low percentage of NBs also expressed Dacapo (Dap, Fig. 2D, D'), the ortholog of p21/p27 in flies that negatively regulates the G1-S transition [21]. However, co-depletion of Dap did not restore the number of Pros+ cells or the size of the brain (Fig. 2D'), thereby pointing to irreversible cell cycle arrest in SAC-depleted NBs. All these data indicate that reduced proliferation of NBs contribute to CIN-induced microcephaly.

Single aneuploidies have a minor effect on NSC number and proliferative capacity

The observation that the effects of SAC depletion on NB number required at least 48 h (Fig. 1A, A' and Supplementary Fig. 1E, E'), despite the rapid cell cycles of this population (every 2 h [18]), pointed

to a delayed response of these cells to aneuploidy [14]. Alternatively, this observation might suggest that NB loss and cycle arrest is a result of a high level of CIN-induced aneuploidy or DNA damage accumulated through consecutive cell cycles. We thus analyzed, in this and the following section, the contribution of different types of aneuploidy and DNA damage to the observed phenotypes. In *Drosophila*, systemic aneuploidies based on trisomies for the X chromosome or the left arm of chromosome II (2L) give rise to mature larvae or pupae that are not able to hatch as adults [22,23]. Trisomic larvae were generated by crossing females bearing a compound X-chromosome (consisting of two attached X chromosomes that segregate together) or a compound-2L (consisting of two attached 2L arms that segregate together and two free 2R arms) with wild-type males carrying an ubiquitously expressed *GFP* transgene on the X or second chromosomes, respectively, thus labeling trisomic female larvae by the expression of the GFP marker. Trisomies for the X and 2L chromosomes were very stable in larval brains, as shown by the presence of the GFP-expressing chromosome in all cells of the central brain (Fig. 3A, B). Based on the developmental delay of trisomic larvae, we quantified the number of NBs and Pros+ cells, as well as brain size throughout the extended larval period and compared these numbers with two types of control euploid larvae, namely those bearing the compound chromosomes and those bearing two unattached chromosomes. The number of NBs was either mildly reduced in the case of X-trisomies (Fig. 3A') or largely unaffected in the case of 2L-trisomies (Fig. 3B'). Although NB proliferation (monitored by the number of Pros+ cells at different developmental points) was delayed in trisomic animals when compared to the two controls, the final number of Pros+ cells at the end of the larval period was largely unaffected (Fig. 3A, A', B, B'). A similar trend was observed for brain size (Fig. 3A, A', B, B'). However, brains trisomic for the X chromosome were still smaller than the control brains at the end of the larval period, pointing to the presence of X chromosome-linked triplosensitive loci affecting the growth of other regions of the brain. All these data indicate that trisomies for the X chromosome and 2L arm have a minor impact on NB viability and proliferative capacity, despite the high number of protein-encoding genes that are potentially unbalanced in trisomics for the X (2196 genes) and 2L chromosomes (2657 genes).

The presence of a single X chromosome in *Drosophila* males causes an imbalance between X-linked and autosomal genes, which is solved by the dosage compensation mechanism (Supplementary Fig.

2A). The Male-Specific Lethal complex, which can be visualized in male tissues by the expression of the Msl2 protein (Supplementary Fig. 2B), targets the X chromosome in males, leading to de-compaction of the chromatin fiber and increased gene transcription to a similar level to that observed in autosomal chromosomes. In females, RNA binding protein Sex lethal (Sxl) induces the translational repression of Msl2 (Supplementary Fig. 2A, B, [24]). Experimental depletion of Msl2 and Sxl in male and female tissues, respectively, causes an X chromosome-wide gene expression imbalance with respect to autosomes (Supplementary Fig. 2C, [25,26]). In contrast to the deleterious effects of these manipulations on the growth and development of epithelial tissues in *Drosophila* [27], the number of NBs was largely unaffected upon Msl2 depletion in males or Sxl depletion in females (Supplementary Fig. 2D). These results reinforce the conclusion regarding the minor impact of single trisomies and their resulting gene dosage imbalance on NB viability and extend this conclusion to single monosomies (in terms of gene expression) caused by Msl2 depletion in male brains.

DNA damage has a delayed impact on NSC number and proliferative capacity

Lagging chromosomes are frequent in cells with SAC defects and are likely to be damaged [28]. Consequently, the DNA damage response (DDR) pathway can be activated [29]. Interestingly, SAC-depleted NBs showed increased levels of phosphorylated H2Av (pH2Av, a target of ATM and ATR in flies [30]), and activation of p53 (monitored by a GFP activity sensor [31], Fig. 4A). However, depletion of DDR genes [*Dp53*, *ATR* (*mei41* in flies*)* or *chk1* (*grapes* in flies)] by RNAi or the use of a dominant negative form of Dp53 (eg. $Dp53^{H159N}$) did not have a major impact on the number of SAC-depleted NBs, and gave rise only to a modest reduction in the size of CIN brains (Fig. 4B, B'). Depletion of DDR genes alone did not cause any major effect on brain size or NB number (Fig. 4B, B'). To further address the contribution of DNA damage to the observed CIN-induced phenotype, we examined whether DNA damage caused by high doses of ionizing radiation (X-ray, IR, 4500 rads) would phenocopy the CIN-induced reduction in the number of NBs or their progeny, as well as the decrease in brain size. Despite strong activation of the DDR pathway, monitored by increased levels of pH2Av in larval brains 5 h after IR, cell death (monitored with an antibody against the cleaved form of the effector Caspase Dcp1, cDcp1), NB number, and mitotic activity were largely unaffected when compared to control non-irradiated brains (Fig. 4C, C'). In contrast, epithelial cells of the larval wing

primordium subjected to a similar dose of IR showed high levels of cDcp1 and low mitotic activity 5 h after exposure (Supplementary Fig. 3A-C). cDcp1 and mitotic activity in the wing primordium were restored to control levels 3 days after IR exposure (Supplementary Fig. 3A-C). However, the number of NBs and Pros+ cells was clearly reduced 3 days after IR exposure, at a time at which pH2Av levels were reduced to those of control brains (Fig. 4C, C', D, D', see also [32]). The temporal delay observed between H2Av phosphorylation, which marks the presence of double-strand breaks (DSBs), and loss of NBs and reduction in the number of Pros+ cells suggests that these phenotypes are an indirect consequence of the presence of DSBs in the tissue, whereby unrepaired DNA would cause genome rearrangements and aneuploidy. Fluorescence in situ hybridization (FISH) analysis of NBs 3 days after IR to count the number of copies of chromosome II revealed a clear increase in the percentage of NBs losing or gaining at least one chromosome (Fig. 4E, E', note that fly chromosomes in interphase are closely attached in normal conditions, thus the presence of a single chromosome in control NBs). These data suggest that the delayed impact of DNA damage to the brain phenotype relies on the production of aneuploid karyotypes, and they point to a role of DNA damage in enhancing aneuploidy levels in CIN brains rather than an immediate effect on the viability or proliferative capacity of NBs.

Our experimental data on the minor effects of simple aneuploidies on NB viability and proliferative capacity (Fig. 3 and Supplementary Fig. 4) and on the proposed effects of DNA damage in enhancing the aneuploidy levels of CIN brains (Fig. 4) point to complex aneuploidies, consisting of multiple losses and gains of chromosomes, as those responsible for NB loss, cell cycle arrest, and CIN-induced microcephaly. Consistently, FISH analysis of NBs to count the number of copies of chromosomes II and III revealed an increase throughout larval development in the percentage of NBs losing or gaining at least one chromosome upon chronic induction of CIN (Fig. 4F, F', see also Supplementary Fig. 1B, B'). Moreover, by using two distinct FISH probes to label chromosomes II and III, we observed that most NBs (18/19) accumulated more than one chromosome and showed an imbalanced number of chromosomes. This finding points to this imbalance as the major contributor of CIN-induced microcephaly (Fig. 4F). These results support the proposal that complex aneuploidies

accumulated through consecutive cell cycles and consisting of multiple gains and losses of chromosomes exert a negative impact on NB number and proliferative capacity.

CIN induces a transcriptional response in developing brains

To identify the molecular mechanisms underlying the negative impact of complex aneuploidies on NB number and proliferation, we characterized the transcriptional profile of brains subjected to chronic depletion of the SAC gene *bub3* and compared it with that of control brains. Among the most upregulated genes (>1.5 fold, 28 genes, Supplementary Data 1) in CIN brains, we observed the presence of four members of the Heat Shock Protein 70 (Hsp70) superfamily of chaperones (*hsp70Ba*, *hsp70Bb*, *hsp70Bc*, and *hsp70Bbb*, Fig. 5A), mediating protein folding, and Glutathione S transferase E8, which belongs to a protein family involved in ROS scavenging. Gene set enrichment analysis also pinpointed genes involved in vesicle trafficking, autophagy, mitophagy, and protein folding as classes of genes whose expression profiles were also significantly upregulated in CIN brains (Fig. 5C, D, and Supplementary Fig. 4B, see also Supplementary Data 2 and 3). Among the most downregulated genes (>1.4 fold, 33 genes, Supplementary Data 1) in CIN brains, we found genes encoding transcription factors involved in neuronal or glial specification, including, as expected, *prospero* (e.g., *castor*, *datilografo*, *huckebein*, *bric a brac 1*), genes involved in mitochondrial homeostasis (e.g., *dj-1beta* [33,34]) and *bub3* (Fig. 5A and Supplementary Data 1). Gene set enrichment analysis also highlighted genes involved in RNA metabolism, nucleolar function, and mitochondrial ribosomes as classes whose expression profiles were also significantly downregulated in CIN brains (Fig. 5C, D, and Supplementary Fig. 4B, see also Supplementary Data 2 and 3). Interestingly, the overall transcriptional profile of the mitochondrial genome was also reduced in these brains (Fig. 5B). The transcriptional response of developing brains to the generation of complex aneuploidies was not reproduced by simple aneuploidies. On one hand, when comparing the changes in gene expression caused by CIN or by trisomies for the X or 2L chromosomes, the observed patterns of upregulation and downregulation showed mild but significant negative correlations (Supplementary Fig. 5A). On other hand, gene set enrichment analysis of brains trisomic for the X or 2L chromosomes did not recapitulate any of the gene classes pinpointed in brains subjected to CIN (Supplementary Fig. 5B). All these results point to a reduction in translation (e.g., ribosome biogenesis) and RNA metabolism,

activation of protein quality control mechanisms (autophagy), and repression of mitochondria activity as the major responses of developing brains to complex aneuploidies. We next validated some of these responses by immunochemistry or the use of activity reporters and characterized their functional contribution to the deleterious effects of complex aneuploidies on NBs.

Aneuploidy induces loss of stemness in NSCs

In developing NBs, ribosome biogenesis in the nucleolus relies on the activity of the dMyc proto-oncogene, which contributes to their enlarged cell and nuclear size [35]. Consistent with the observed transcriptional reduction in nucleolar protein-encoding genes in CIN brains (Fig. 5C, D), a large proportion of aneuploid NBs lost dMyc expression, showed reduced levels of Fibrilarin (a nucleolar protein involved in RNA processing and regulated by dMyc [36,37]), and were small (Fig. 5E, E'). dMyc also plays an important role in conferring NB identity by maintaining cortical polarity, a requirement for the intrinsic capacity of NBs to divide asymmetrically and avoid the nuclear entry of the transcription factor Prospero [35]. Consistently, a proportion of aneuploid NBs showed nuclear localization of Prospero (Fig. 5E, E', see also [13,14]), and, most interestingly, aneuploid NBs frequently lost the expression of Dpn or Worniu (Fig. 5E, E'), two transcription factors involved in promoting NB self-renewal through asymmetric cell division and avoiding premature differentiation [38,39]. All these observations indicate that the aneuploidy-induced reduction in NB number and proliferative capacity is most probably a result of loss of stemness. Overexpression of dMyc or Worniu did not block the elimination of aneuploid NBs (Fig. 5E''). Only Worniu, when overexpressed, was able to partially rescue the number of Prospero-positive cells in CIN brains (Fig. 5E''), most probably through its role in driving NB cell cycle progression [38]. Neither did depletion of the pro-differentiation transcription factor Prospero (Pros) rescue the reduction in the number of aneuploid NBs caused by CIN (Fig. 5E''). Apoptosis has alternatively been proposed to play a role in the reduction in brain size caused by changes in centrosome number and SAC depletion [15]. To quantify the levels of apoptosis in NBs subjected to *bub3* depletion, we monitored activation of the apoptotic machinery with an antibody that detects the cleaved form of the effector Caspase Dcp1 (cDcp1) and an activity reporter of effector Caspases Dcp1 and Drice that becomes fluorescent upon caspase-driven cleavage (GC3Ai [40]) Whereas the percentage of control NBs positive for either of these two markers remained close to

zero throughout larval development, a low but significant percentage of NBs subjected to CIN were positively labeled by these markers (Supplementary Fig. 4C, C''). Inhibition of apoptosis with the baculovirus protein p35, an inhibitor of effector caspases in *Drosophila*, restored the number of NBs subjected to CIN only at early stages of development. However, the dramatic reduction in NB number in mature brains was still observed (Supplementary Fig. 4C'', see also [13]). All these results indicate that the aneuploidy-induced loss of NB identity and proliferative capacity is a consequence of loss of stemness but not cell death or premature differentiation, as previously proposed [13,15]. Consistent with this notion, *prospero* depletion combined with apoptosis inhibition did not rescue the dramatic reduction in NB number in mature brains subjected to CIN either (Supplementary Fig. 4D, D'). We then addressed whether the loss of stemness - a highly energy demanding cellular state - observed in highly aneuploid NSCs is caused by proteostasis failure and mitochondrial dysfunction.

Proteostasis failure and mitochondrial dysfunction contribute to the loss of stemness

As a follow-up of the identification of a general upregulation of genes involved in protein folding, vesicle trafficking and autophagy in CIN brains, by mean of RNAseq, we next monitored the activity of the two main protein quality control mechanisms, namely the ubiquitin-proteasome system (UPS) and autophagy, in aneuploid NBs. To characterize the *in vivo* activity of the proteasome in these cells, we used CL1-GFP, a fusion protein created by attaching a proteasome degradation signal to GFP [41]. Whereas CL1-GFP was rapidly degraded in control NBs and no accumulation was observed, this protein accumulated in aneuploid NBs (Fig. 6A), pointing to a situation of near saturation of the proteasome in these cells. To reinforce this notion, we used Htt25Q, a fusion protein consisting of human Huntingtin with a polyQ stretch containing only 25 glutamines and fused to a Cerulean fluorescent protein [42]. Htt25Q does not form aggregates nor does it cause toxicity on its own. However, the presence of protein aggregates in the cell can seed Htt25Q polymerization [43]. Whereas Htt25Q showed diffuse expression in control NBs (Fig. 6B) and did not alter the number of NBs (Fig. 6D and Supplementary Fig. 6B), it accumulated in large foci in aneuploid NBs (Fig. 6B) and caused a further reduction in the size of this population (Fig. 6D and Supplementary Fig. 6B). Together with the UPS, autophagy—a pathway responsible for the lysosomal degradation of cellular components—plays an essential role in maintaining protein homeostasis (proteostasis). High levels of autophagy

were induced in aneuploid NBs, as visualized by the punctated accumulation of ChAtg8a (a mCherry-tagged form of Atg8a, which becomes membrane-associated under autophagy induction and localizes to the site of autophagosome nucleation [44]) in these cells (Fig. 6C). In control brains, small Atg8a-positive puncta were observed only in small cells around the NBs but never in the NBs themselves (Fig. 6C, arrowheads). Interestingly, boosting autophagy (by overexpressing Atg1 or depleting the activity of Tor through Rheb depletion or the use of Tor mutants in heterozygosis) led to a significant rescue of the number of aneuploid NBs in mature CIN brains, without causing any major effect in otherwise control brains (Fig. 6D and Supplementary Fig. 6A). A similar result was obtained by feeding larvae with the TOR inhibitor Rapamycin (Supplementary Fig. 6C). These results indicate that proteostasis failure, most probably due to an imbalance in the proteome caused by aneuploidy, functionally contributes to the reduction in the number of NBs in CIN brains. However, we noticed that none of the genetic interventions aimed at increasing autophagy was able to rescue the number of Pros+ cells or the size of the larval brain (Fig. 6E and Supplementary Fig. 6C). These results suggest that TOR inhibition or non-physiological levels of autophagy might have a negative impact on the proliferative capacity of highly aneuploid NBs.

The transcriptional upregulation of genes involved in mitochondrial disassembly and the transcriptional downregulation of genes encoding mitochondrial ribosome components (Fig. 5C), together with the reduction in overall mitochondrial transcription (Fig. 5B), pointed to a negative impact of aneuploidy on mitochondrial number or function. The developing brain is characterized by NBs strongly enriched by mitochondria surrounding the centrally localized nucleus (Fig. 7A, B). In aneuploid NBs, we observed large accumulations of mitochondria that were not equally distributed around the nucleus (Fig. 7A, B). Using a MitoTimer reporter, which targets the oxidation-sensitive Timer protein to mitochondria [45], we detected a shift of mitochondrial fluorescence toward red in aneuploid NBs (Fig. 7C), which points either to high rates of mitochondrial oxidation or slow rates of mitochondrial turnover. We then used MitoQC [46], where a tandem GFP-mCherry fusion protein is targeted to the outer mitochondrial membrane, to analyze mitophagy, an important quality control mechanism that removes damaged mitochondria, in CIN brains. MitoQC exploits the pH sensitivity of GFP to enable differential labeling of mitochondria in the acidic microenvironment of the lysosome as

a proxy endpoint readout. Only a few small MitoQC-positive puncta, most of them red, marking mitolysosomes, were observed in progeny cells of control brains (Fig. 7D, arrowheads). In contrast, large MitoQC-positive accumulations were observed in aneuploid NBs, and most (if not all) were positive for both colors (Fig. 7D). We support the proposal that near saturation of autophagy compromises mitophagic activity, thus leading to the accumulation of dysfunctional mitochondria in aneuploid NBs. Consistent with this, overexpression of mitochondria-specific chaperones Hsp60 and Hsp60c, or ROS scavengers Sod2 and GTPx-1 was able to significantly rescue the number of aneuploid NBs observed in mature CIN brains, without causing any major effect in otherwise control brains (Fig. 7E and Supplementary Fig. 7A). These genetic interventions also rescued the number of Pros+ cells (Fig. 7E) and, most interestingly, yielded a complete restoration of brain size (Fig. 7G and Supplementary Fig. 7A). The observation that overexpression of ROS scavengers and mitochondrial chaperones in NB cells fully restored brain size, but only partially NB cell counts, points to a role of mitochondrial dysfunction in compromising not only the fitness but also the mitotic activity of highly aneuploid NBs. Alternatively, these genetic interventions might target, through perdurance of the proteins that are overexpressed, the progeny cells thus restoring their fitness. Notably, the inhibition of apoptosis through p35 expression rescued the number of Pros+ cells and resulted in a complete restoration of brain size (Supplementary Fig. 4C'' and Supplementary Fig. 7B), despite no concomitant rescue of NB numbers. These findings can be explained by inheritance of p35 by progeny cells and points to a role of apoptosis in the elimination of these cells.

Discussion

Mosaic variegated aneuploidy (MVA), a rare human disease that consists of widespread mosaic aneuploidies, is characterized by severe microcephaly [1–4]. MVAs is caused by single mutations in genes involved in accurate segregation of chromosomes during mitosis [5–10]. Here we generated a *Drosophila* model of MVA-driven microcephaly by targeting the SAC genes *bub3* or *rod* specifically in the neural stem cell (NSC) compartment. We present evidence that loss of stemness—reduced viability and proliferative capacity—of SAC-depleted NSCs contributes to MVA-driven microcephaly and that it results in a lower number of neurons and glial cells. Using this model, we present evidence

362 that it is the accumulation of complex aneuploidies (an unbalanced number of gains and losses of
363 more than one chromosome) over time rather than a direct consequence of DNA damage or simple
364 aneuploidies what compromises the identity and proliferative capacity of NSCs. This conclusion is
365 consistent with previous reports unraveling a delayed response of NSCs to acute depletion of the
366 cohesin complex, also known to cause CIN [14]. Thus, neither DNA damage caused by acute ionizing
367 radiation had any impact on NSC identity or proliferative capacity, nor did the depletion of genes
368 involved in the DNA damage response pathway strongly enhance the deleterious effects of SAC
369 depletion on brain development. Similarly, despite the growth retardation observed in the developing
370 brains of flies trisomic for the X and 2L chromosomes (carrying more than 2000 genes each), the
371 number and proliferative activity of their NSCs were largely unaffected. Although highly aneuploid
372 NSCs tended to express pro-differentiation factors, probably as a result of their identity loss, and
373 some even activated the apoptotic pathway, their loss was neither a direct consequence of cell death
374 nor a result of premature differentiation, as previously proposed [13,15]. Indeed, our transcriptomic
375 analysis unveiled a strong effect of CIN on cellular homeostasis. Thus, the major responses of
376 developing brains to CIN-induced complex aneuploidies included a reduction in genes involved in
377 ribosome biogenesis and RNA metabolism, activation of protein quality control mechanisms
378 (autophagy), and repression of mitochondrial activity. These transcriptomic changes are consistent
379 with the conserved impact of aneuploidy on proteostasis [47–49] and mitochondrial health [50]. Thus, in
380 yeast and human cells, aneuploidy leads to the production of an unbalanced proteome, which causes
381 proteotoxic stress and activation of the major quality control mechanisms, including autophagy. Near
382 saturation of autophagy in aneuploid cells has been demonstrated to compromise mitophagy, thus
383 leading to the accumulation of dysfunctional mitochondria, which produce radical oxygen species
384 (ROS). Consistent with the observed transcriptomic changes, highly aneuploid NSCs showed
385 reduced expression of dMyc (a major regulator of ribosome biogenesis in vertebrates and
386 invertebrates [51,52]) and smaller nucleoli, near saturation of the ubiquitin-proteasome system, strong
387 activation of autophagy, and high sensitivity to protein aggregates. Activation of autophagy in these
388 cells either by overexpression of Atg1 or depletion of TOR was able to partially rescue the reduced
389 number of NSCs observed in SAC-depleted brains. The genetic interventions performed were

unsuccessful in restoring progeny cell numbers or brain size. Future studies are required to ascertain whether TOR inhibition or aberrant autophagy levels negatively impact the proliferative capacity of highly aneuploid NSCs. Mitophagy was largely compromised in highly aneuploid NSCs, which also showed large accumulations of mitochondria not equally distributed around the nucleus. Overexpression of mitochondrial chaperones or ROS scavengers also partially restored the aneuploid NB count observed in mature CIN brains. We noticed that the number of aneuploid NBs was not fully rescued by any of these genetic interventions, most probably as a result of the highly pleiotropic effects of aneuploidy on cell physiology and on the fact that the complete loss of chromosomes is incompatible with cell viability. By contrast, overexpression of mitochondrial chaperones or ROS scavengers significantly rescued the number of progeny cells and fully restored brain size. To our surprise, inhibition of apoptosis through p35 expression also resulted in a complete restoration of brain size and partial rescue of progeny cell number, despite no concomitant rescue of NB numbers, pointing to a role of apoptosis in the elimination of progeny cells most probably as a consequence of the generation of aneuploid karyotypes. Thus, genetic interventions aimed at restoring mitochondria homeostasis or blocking apoptosis will undoubtedly offer new opportunities for drug discovery and disease treatment. The experimental observations that these genetic interventions rescue brain size without fully rescuing NSC numbers point to existing homeostatic mechanisms aimed at restoring brain size in a situation of NSC depletion. Whether these homeostatic mechanisms rely on the ability of progeny cells to over proliferate in order to restore the final number of neurons and glial cells remains to be elucidated. Taken together, our data indicate that CIN-induced microcephaly stems, on one hand, from the generation, over time and through consecutive cell cycles, of NSCs carrying highly complex aneuploid karyotypes (Fig. 7F). Complex aneuploidies compromise the highly energy-demanding stemness of NSCs – their stem cell identity and proliferative capacity- by causing proteostasis failure and mitochondrial dysfunction. On other hand, the ultimate effect of CIN on brain size also stems from the apoptotic elimination of progeny cells, most probably as a direct consequence of aneuploidy.

Methods

418 **Fly maintenance, husbandry and transgene expression**

419 Strains of *Drosophila melanogaster* were maintained on standard medium (4% glucose, 55 g/L yeast,
420 0.65% agar, 28 g/L wheat flour, 4 ml/L propionic acid and 1.1 g/L nipagin) at 25°C in light/dark cycles
421 of 12 h. When not specified, the sex of experimental larvae was not considered relevant to this study
422 and was not determined. The strains used in this study are summarized in Supplementary Data 4.
423 Research in *Drosophila* is not subject to animal experimentation regulations. All experiments were
424 performed in both sexes, except those altering Sxl or Msl2, which inherently have sex-specific roles
425 and so were treated separately by sex.

426 **Standard induction of CIN and gene expression**

427 Virgin female flies carrying the *wor-GAL4* driver and *UAS-bub3-i* were crossed with male flies
428 carrying the gene of interest for each experiment. Fertilized females were allowed to lay eggs at 25°C
429 and the resulting larvae were switched to 29°C 3 h after egg laying (AEL) in time point experiments,
430 and 8 h AEL for the rest of the experiments. Brains were dissected after 48, 62, 72 or 96 h AEL. Both
431 female and male larvae were used, except when characterizing Sxl and Msl2, in which females and
432 males were considered separately. *UAS-gfp-RNAi* was used as a control for those experimental UAS
433 transgenes targeting the corresponding pathways or genes. When using the Gal80ts system, flies
434 and their progeny were maintained at 18ºC to keep GAL4/UAS suppressed, and shifted to 29ºC to
435 inactivate the temperature-sensitive Gal80ts form and activate the GAL4/UAS system.

436 **Pupariation assays**

437 Flies were allowed to lay eggs for 4 h at 25°C after which they were switched to 29ºC. Hatching larvae
438 were counted. Number of pupae was scored always at the same time point and 24h apart. The
439 experiment was performed in four replicates, and the resulting percentage of pupae was calculated with
440 respect to the total number of larvae that hatched (47 larvae in the control group and 35 in experimental
441 group) or the total number of larvae that survived until pupal stages (47 larvae in the control group and
442 30 in experimental group).

443 **Rapamycin treatment**

Flies of interest were crossed and allowed to lay eggs for 12 h at 25ºC. Larvae were then kept for 48 h AEL at 25ºC before being shifted to 29ºC for 24 h. Afterwards, rapamycin was added to reach a final concentration of 40 µM, while controls received DMSO at a final concentration of 0.4%. Larvae were maintained for approximately 48 h more at 29ºC and then dissected.

Colchicine assay

Flies of interest were crossed and allowed to lay eggs for 24 h at 18ºC. Larvae were maintained at 18ºC during development, except for the last 24 h, when they were shifted to 29ºC to inactivate the Gal80ts and thus permit activation of the GAL4/UAS system. Larvae were dissected and incubated with 50 µM colchicine for experimental condition and 0.05% DMSO for controls for 4 h at 25°C in Schneider's media (Sigma-Aldrich) supplemented with 10% fetal bovine serum (Invitrogen) before immunostaining.

Irradiation

Whole wild-type larvae were X-irradiated with 4500 rads in an YXLON MaxiShot X-ray system. Larval brains and wing discs were dissected and analyzed at the indicated time points after the irradiation.

Chromosome labeling by FISH

Fluorescence in situ DNA hybridization (FISH) was carried out to label the 2nd and 3rd chromosomes in brain cells. Briefly, larval brains were dissected in cold PBS and fixed with 4% paraformaldehyde for 20 min. Fixed tissues were washed with PBS-Tr (PBS1X; 0.3% Triton X-100) and transferred gradually into pre-Hybridization Mixture (pHM) (50% formamide; 4X SSC; 100mM NaH2PO4 pH7; 0.1% Tween 20). 150 ng of AACAC(2nd) -Alexa 488 -$(AACAC)_6$) [53]and dodeca (3rd)-Alexa 488-CCCGTACTGGTCCCGTACTGGT [54] chromosome probes were added and probe/chromosomal DNA was denatured by heating the sample to 91°C for 5 min. Hybridization was performed at 37°C overnight. After post-hybridization washes, brains were blocked and incubated overnight at 4°C in PBS-Tr; 10% Normal Goat Serum (NGS) with the primary antibody (anti-DPN). DAPI was used to counterstain DNA. Confocal sections covering the entire nuclei were taken and analyzed using Fiji Software (NIH, USA).

Immunohistochemistry

Larvae of interest were selected, and brains were dissected in phosphate-buffered saline (PBS), fixed for 20 min in 4% formaldehyde in PBS, and stained with antibodies in PBS with 0.3% BSA and 0.2% Triton X-100. Primary and secondary antibodies are summarized in the Supplementary Data 4.

DNA synthesis

Click-iT™ Plus EdU Alexa Fluor™ 647 Imaging Kit from Invitrogen (C10640) was used to measure DNA synthesis (S phase) in proliferating cells, following the manufacturer's indications. EdU (5-ethynyl-2´-deoxyuridine) provided in the kit is a nucleoside analog of thymidine and is incorporated into DNA during active DNA synthesis. Larval brains were incubated with EdU for 20 min and then permeabilized in PBT of 40 min. The samples were incubated with the Click-iT reaction cocktails for 45 min at room temperature.

Generation of trisomic larvae

To generate trisomic larvae for the X chromosome*, C(1)DX, y* virgin females were crossed with *GFP-FRT18A* males (see Supplementary Data 4). Trisomic X female larvae were identified based on the absence of testes and the presence of GFP. To generate trisomic larvae for the 2L chromosome, *C(2L)SH1* virgin females were crossed with Oregon R males (see Supplementary Data 4). This cross produces both monosomic and trisomic embryos for the 2L chromosome. However, monosomic embryos do not survive past embryogenesis, ensuring that all larvae in the progeny are trisomic and available for dissection.

RNAseq library preparation

The samples used for this study were late third instar (L3) larvae from *Drosophila* (96 h AEL). The genotypes of control larvae were (i) *w; worniu-gal4, uas-gfp-RNAi*; (ii) *C(1)DX/Y;* and *(iii)C(2L)SH1*, while the genotypes of the experimental larvae were (i) *w; worniu-gal4, uas-bub3-RNAi;* (ii) *C(1)DX/X* (trisomic for the X chromosome) and (iii) *C(2L)SH1*/+ (trisomic for the 2L chromosome). Three independent biological replicates were performed on different days, with three brains dissected per genotype and replicate. All larvae used in these experiments were female. The brains were collected in 45 µl of lysis buffer containing 20 mM DTT, 10 mM Tris-HCl pH 7.4, 0.5% SDS, and 0.5µg/µl

proteinase K, incubated at 65 ºC for 15 min, and immediately frozen until processing. RNA isolation and library preparation were done at the IRB Barcelona Functional Genomics Core Facility. RNA was treated with DNAse I and purified using magnetic beads (RNAClean XP, Beckman Coulter). RNA quantity was measured with the Qubit RNA HS Assay kit (Invitrogen), and integrity was assessed with the Bioanalyzer 2100 RNA Pico assay (Agilent). Poly-A mRNA was purified from 150 ng of total RNA using the kit NEBNext Poly(A) mRNA Magnetic Isolation Module (New England Biolabs). Dual-indexed cDNA libraries were generated using the NEBNext Ultra II RNA Library Prep Kit for Illumina (New England Biolabs). All libraries underwent 13 min of RNA fragmentation and 13 cycles of PCR amplification. The final libraries were quantified using the Qubit dsDNA HS assay (Invitrogen) and subjected to quality control using the Tapestation HS D5000 assay (Agilent). An average size of 380 bp was confirmed. An equimolar pool was prepared with all the libraries for SE50 sequencing on a NextSeq 2000 (Illumina), and at least 26 million reads were obtained for each library.

Data processing

Adapters from reads were removed using trim galore (v.0.6.7) (https://github.com/FelixKrueger/TrimGalore) with default parameters. Resulting reads were aligned to the dm6 *D. melanogaster* genome version using STAR (v.2.7.10a) [55]. The count matrix was generated in R (https://www.R-project.org/) through the function "featureCounts" of the Rsubread package [56].

Differential expression

Differential expression was performed using the DESeq2 package [57]. The function lfcShrink was used to attenuate the influence of low counts in fold changes (FC Shrunk in figures). For plotting purposes and generating principal components, the count matrix was normalized using the "vst" function. In the case of trisomic brains, normalization and DEG analysis was performed chromosome by chromosome.

Gene set enrichment analysis

Gene set enrichment analysis was performed using the roastgsa package [58]. GO and KEGG pathways were downloaded using the org.Dm.eg.db package.

Comparison of DEGs and NES between genotypes

A linear model was fitted to the log2 fold changes of CIN and trisomies. R squared and association p-value are reported. The regression line and the corresponding equation was added to the plot.

Confocal microscopy

Samples were analyzed using the following confocal microscopes: LSM 780 Zeiss and LSM880 Zeiss fitted with a Fast Airyscan module (Carl Zeiss). Z-stacks were acquired using either the laser scanning confocal mode or the High-Resolution mode (Airyscan). Image acquisition was done with 40x and 63x oil lenses. The most representative image is shown in all experiments.

Brain size and cell quantification

Number of NBs was quantified manually using Fiji Software (NIH, USA) according to Dpn staining and nuclear size (>7µm). Only the NBs located in the ventral part of the central brain were taken into consideration. Size of the whole brain lobe, represented as area, was measured manually using Fiji Software on Z stacks obtained using a Zeiss LSM780 confocal microscope at 40x oil immersion objective. The numbers of progeny cells (GMCs, neurons and glia) were determined using IMARIS Software with the 'Spots' tool, according to Pros, Elav or Repo staining, respectively. Areas of G-TRACE and Ph2Av were measured with IMARIS software using the 'Surface' tool. *UAS-gfp-RNAi* was used as a control for those experimental UAS transgenes targeting the corresponding pathways or genes.

Statistical analysis and reproducibility

Statistical analysis was performed by unpaired equal-variance two-tail Student's t-test when comparing the difference in means between two groups. We used a one-way ANOVA to compare three or more groups within the same experiment. In contrast, a two-way ANOVA was employed when there were multiple comparisons across different groups at various time points. Results for

pairwise comparisons were adjusted by multiple contrasts using Tukey/Šídák correction, depending on the experiment (details in figures and Supplementary Data 4). Differences were considered significant when p values were less than 0.0001 (****), 0.001 (***), 0.01 (**), or 0.05 (*). All genotypes included in each histogram or scatter plot were subjected to the same experimental conditions (temperature and time of transgene induction) and analyzed in parallel. Mean values and standard deviations were calculated and the corresponding statistical analysis and graphical representations were carried out with GraphPad Prism 10 statistical software. All quantifications were carried out in at least two independent replicates per genotype. Representative micrographs shown in all figures are based on at least 10 different brains per genotype and experimental condition.

Data availability

Materials generated for the study are available from the corresponding author on request. The raw and processed RNAseq data have been deposited in the GEO database under accession numbers GSE290206 (CIN data) and GSE301548 (trisomies data). Source data are provided with this paper in Source Data File.

References

1. García-Castillo, H., Vásquez-Velásquez, A. I., Rivera, H. & Barros-Núñez, P. Clinical and genetic heterogeneity in patients with mosaic variegated aneuploidy: Delineation of clinical subtypes. *Am. J. Med. Genet. Part A* **146A**, 1687–1695 (2008).

2. Suijkerbuijk, S. J. E. *et al.* Molecular Causes for BUBR1 Dysfunction in the Human Cancer Predisposition Syndrome Mosaic Variegated Aneuploidy. *Cancer Res.* **70**, 4891–4900 (2010).

3. Pavone, P. *et al.* Pathogenic correlation between mosaic variegated aneuploidy 1 (MVA1) and a novel BUB1B variant: a reappraisal of a severe syndrome. *Neurol. Sci.* **43**, 6529–6538

(2022).

4. Malumbres, M. & Villarroya-Beltri, C. Mosaic variegated aneuploidy in development, ageing and cancer. *Nat. Rev. Genet.* **25**, 864–878 (2024).

5. Matsuura, S. *et al.* MonoallelicBUB1B mutations and defective mitotic-spindle checkpoint in seven families with premature chromatid separation (PCS) syndrome. *Am. J. Med. Genet. Part A* **140A**, 358–367 (2006).

6. Hanks, S. *et al.* Constitutional aneuploidy and cancer predisposition caused by biallelic mutations in BUB1B. *Nat Genet* **36**, 1159–1161 (2004).

7. de Wolf, B. *et al.* Chromosomal instability by mutations in the novel minor spliceosome component CENATAC. *EMBO J.* **40**, (2021).

8. Langeh, N. *et al.* Mosaic variegated aneuploidy syndrome 2 with biallelic novel CEP57 splice site variation in Indian siblings: Expanding the clinical and molecular spectrum. *Clin. Genet.* **103**, 478–483 (2023).

9. Yost, S. *et al.* Biallelic TRIP13 mutations predispose to Wilms tumor and chromosome missegregation. *Nat. Genet.* **49**, 1148–1151 (2017).

10. Carvalhal, S. *et al.* Biallelic BUB1 mutations cause microcephaly, developmental delay, and variable effects on cohesion and chromosome segregation. *Sci. Adv.* **8**, (2022).

11. Okimoto, R. A. *et al.* Inactivation of Capicua drives cancer metastasis. *Nat Genet* **49**, 87–96 (2017).

12. Sterling, N. A., Terry, B. K., McDonnell, J. M. & Kim, S. P53 independent pathogenic mechanisms contribute to BubR1 microcephaly. *Front. Cell Dev. Biol.* **11**, (2023).

13. Gogendeau, D. *et al.* Aneuploidy causes premature differentiation of neural and intestinal stem cells. *Nat Commun* **6**, 8894 (2015).

14. Mirkovic, M., Guilgur, L. G., Tavares, A., Passagem-Santos, D. & Oliveira, R. A. Induced

595 aneuploidy in neural stem cells triggers a delayed stress response and impairs adult life
596 span in flies. *PLOS Biol.* **17**, e3000016 (2019).

597 15. Poulton, J. S., Cuningham, J. C. & Peifer, M. Centrosome and spindle assembly checkpoint
598 loss leads to neural apoptosis and reduced brain size. *J. Cell Biol.* **216**, 1255–1265 (2017).

599 16. Homem, C. C. F., Repic, M. & Knoblich, J. A. Proliferation control in neural stem and
600 progenitor cells. *Nat. Rev. Neurosci.* **16**, 647–659 (2015).

601 17. Shiga, Y., Tanaka-Matakatsu, M. & Hayashi, S. A nuclear GFP/β-galactosidase fusion
602 protein as a marker for morphogenesis in living Drosophila. *Dev. Growth Differ.* **38**, 99–106
603 (1996).

604 18. Ito, K. & Hotta, Y. Proliferation pattern of postembryonic neuroblasts in the brain of
605 Drosophila melanogaster. *Dev. Biol.* **149**, 134–148 (1992).

606 19. Evans, C. J. *et al.* G-TRACE: rapid Gal4-based cell lineage analysis in Drosophila. *Nat*
607 *Methods* **6**, 603–605 (2009).

608 20. Zielke, N. *et al.* Fly-FUCCI: A versatile tool for studying cell proliferation in complex tissues.
609 *Cell Rep* **7**, 588–598 (2014).

610 21. de Nooij, J. C., Letendre, M. A. & Hariharan, I. K. A cyclin-dependent kinase inhibitor,
611 Dacapo, is necessary for timely exit from the cell cycle during Drosophila embryogenesis.
612 *Cell* **87**, 1237–1247 (1996).

613 22. Brehme, K. S. Effects of the Triplo-X Condition on Development in Drosophila melanogaster.
614 *Exp. Biol. Med.* **37**, 578–580 (1937).

615 23. Fitz-Earle, M. & Holm, D. G. EXPLORING THE POTENTIAL OF COMPOUND;FREE-ARM
616 COMBINATIONS OF CHROMOSOME 2 IN DROSOPHILA MELANOGASTER FOR
617 INSECT CONTROL AND THE SURVIVAL TO PUPAE OF WHOLE-ARM TRISOMIES.
618 *Genetics* **89**, 499–510 (1978).

619 24. Lucchesi, J. C. & Kuroda, M. I. Dosage Compensation in Drosophila. *Cold Spring Harb.*

Perspect. Biol. **7**, a019398 (2015).

25. Hamada, F. N., Park, P. J., Gordadze, P. R. & Kuroda, M. I. Global regulation of X chromosomal genes by the MSL complex in Drosophila melanogaster. *Genes Dev* **19**, 2289–2294 (2005).

26. Alekseyenko, A. A. *et al.* Sequence-specific targeting of dosage compensation in Drosophila favors an active chromatin context. *PLoS Genet* **8**, e1002646 (2012).

27. Clemente-Ruiz, M. *et al.* Gene Dosage Imbalance Contributes to Chromosomal Instability-Induced Tumorigenesis. *Dev Cell* **36**, 290–302 (2016).

28. Vitre, B. D. & Cleveland, D. W. Centrosomes, chromosome instability (CIN) and aneuploidy. *Curr Opin Cell Biol* **24**, 809–815 (2012).

29. Janssen, A., van der Burg, M., Szuhai, K., Kops, G. J. & Medema, R. H. Chromosome segregation errors as a cause of DNA damage and structural chromosome aberrations. *Science (80-.).* **333**, 1895–1898 (2011).

30. Dekanty, A., Barrio, L., Milán, M. & Milan, M. Contributions of DNA repair, cell cycle checkpoints and cell death to suppressing the DNA damage-induced tumorigenic behavior of Drosophila epithelial cells. *Oncogene* **34**, 978–985 (2015).

31. Zhang, B., Mehrotra, S., Ng, W. L. & Calvi, B. R. Low Levels of p53 Protein and Chromatin Silencing of p53 Target Genes Repress Apoptosis in Drosophila Endocycling Cells. *PLoS Genet.* **10**, e1004581 (2014).

32. Wagle, R. & Song, Y.-H. Ionizing radiation reduces larval brain size by inducing premature differentiation of Drosophila neural stem cells. *Biochem. Biophys. Res. Commun.* **523**, 555–560 (2020).

33. Meulener, M. C., Xu, K., Thomson, L., Ischiropoulos, H. & Bonini, N. M. Mutational analysis of DJ-1 in Drosophila implicates functional inactivation by oxidative damage and aging. *Proc. Natl. Acad. Sci.* **103**, 12517–12522 (2006).

34. De Lazzari, F. *et al.* DJ-1 promotes energy balance by regulating both mitochondrial and autophagic homeostasis. *Neurobiol. Dis.* **176**, 105941 (2023).

35. Rust, K., Tiwari, M. D., Mishra, V. K., Grawe, F. & Wodarz, A. Myc and the Tip60 chromatin remodeling complex control neuroblast maintenance and polarity in Drosophila. *EMBO J.* **37**, (2018).

36. Coller, H. A. *et al.* Expression analysis with oligonucleotide microarrays reveals that MYC regulates genes involved in growth, cell cycle, signaling, and adhesion. *Proc. Natl. Acad. Sci.* **97**, 3260–3265 (2000).

37. Orian, A. *et al.* Genomic binding by the Drosophila Myc, Max, Mad/Mnt transcription factor network. *Genes Dev.* **17**, 1101–1114 (2003).

38. Lai, S.-L., Miller, M. R., Robinson, K. J. & Doe, C. Q. The Snail Family Member Worniu Is Continuously Required in Neuroblasts to Prevent Elav-Induced Premature Differentiation. *Dev. Cell* **23**, 849–857 (2012).

39. San-Juán, B. P. & Baonza, A. The bHLH factor deadpan is a direct target of Notch signaling and regulates neuroblast self-renewal in Drosophila. *Dev. Biol.* **352**, 70–82 (2011).

40. Schott, S. *et al.* A fluorescent toolkit for spatiotemporal tracking of apoptotic cells in living Drosophila tissues. *Development* **144**, 3840–3846 (2017).

41. Pandey, U. B. *et al.* HDAC6 rescues neurodegeneration and provides an essential link between autophagy and the UPS. *Nature* **447**, 859–863 (2007).

42. Ramdzan, Y. M. *et al.* Huntingtin Inclusions Trigger Cellular Quiescence, Deactivate Apoptosis, and Lead to Delayed Necrosis. *Cell Rep.* **19**, 919–927 (2017).

43. Serpionov, G. V., Alexandrov, A. I., Antonenko, Y. N. & Ter-Avanesyan, M. D. A protein polymerization cascade mediates toxicity of non-pathological human huntingtin in yeast. *Sci. Rep.* **5**, 18407 (2016).

44. Hegedűs, K. *et al.* The Ccz1-Mon1-Rab7 module and Rab5 control distinct steps of

autophagy. *Mol. Biol. Cell* **27**, 3132–3142 (2016).

45. Laker, R. C. *et al.* A Novel MitoTimer Reporter Gene for Mitochondrial Content, Structure, Stress, and Damage in Vivo. *J. Biol. Chem.* **289**, 12005–12015 (2014).

46. Lee, J. J. *et al.* Basal mitophagy is widespread in Drosophila but minimally affected by loss of Pink1 or parkin. *J. Cell Biol.* **217**, 1613–1622 (2018).

47. Stingele, S. *et al.* Global analysis of genome, transcriptome and proteome reveals the response to aneuploidy in human cells. *Mol Syst Biol* **8**, 608 (2012).

48. Santaguida, S., Vasile, E., White, E. & Amon, A. Aneuploidy-induced cellular stresses limit autophagic degradation. *Genes Dev* **29**, 2010–2021 (2015).

49. Torres, E. M. *et al.* Effects of aneuploidy on cellular physiology and cell division in haploid yeast. *Science (80-.).* **317**, 916–924 (2007).

50. Joy, J. *et al.* Proteostasis failure and mitochondrial dysfunction leads to aneuploidy-induced senescence. *Dev. Cell* **56**, 2043-2058.e7 (2021).

51. Pierce, S. B. *et al.* Drosophila growth and development in the absence of dMyc and dMnt. *Dev. Biol.* **315**, 303–316 (2008).

52. Popay, T. M. *et al.* MYC regulates ribosome biogenesis and mitochondrial gene expression programs through its interaction with host cell factor–1. *Elife* **10**, (2021).

53. Joyce, E. F., Williams, B. R., Xie, T. & Wu, C. T. Identification of genes that promote or antagonize somatic homolog pairing using a high-throughput FISH-based screen. *PLoS Genet* **8**, e1002667 (2012).

54. Dekanty, A., Barrio, L., Muzzopappa, M., Auer, H. & Milan, M. Aneuploidy-induced delaminating cells drive tumorigenesis in Drosophila epithelia. *Proc Natl Acad Sci U S A* **109**, 20549–20554 (2012).

55. Dobin, A. *et al.* STAR: ultrafast universal RNA-seq aligner. *Bioinformatics* **29**, 15–21 (2013).

56. Liao, Y., Smyth, G. K. & Shi, W. The R package Rsubread is easier, faster, cheaper and better for alignment and quantification of RNA sequencing reads. *Nucleic Acids Res.* **47**, e47–e47 (2019).

57. Love, M. I., Huber, W. & Anders, S. Moderated estimation of fold change and dispersion for RNA-seq data with DESeq2. *Genome Biol.* **15**, 550 (2014).

58. Caballé-Mestres, A., Berenguer-Llergo, A. & Stephan-Otto Attolini, C. Roastgsa: a comparison of rotation-based scores for gene set enrichment analysis. *BMC Bioinformatics* **24**, 408 (2023).

Acknowledgments

We thank E. Baehrecke, G. Juhász, N. Perrimon, J. B. Skeath, M. Suzanne, A. Whitworth, the Bloomington *Drosophila* Stock Center (USA), the Vienna Drosophila Resource Center (Austria), Kyoto Drosophila Stock Center (Japan), and the Developmental Studies Hybridoma Bank (USA) for flies and antibodies, and IRB Barcelona's Advanced Digital Microscopy, Functional Genomics and Biostastics/Bioinformatics Facilities for help. This work was funded by the PID2019-110082GB-I00 and PID2022-137673NB-I00 grants from the Spanish Ministry of Science, Innovation and Universities, and the ERDF "Una manera de hacer Europa". We gratefully acknowledge institutional funding from the Spanish Ministry of Science, Innovation and Universities through the Centres of Excellence Severo Ochoa Award, and from the CERCA Programme of the Catalan Government.

Author Contributions Statement

All authors conceived and designed the experiments and analyzed the data, AG-B, AAH and DB performed the experiments, J.J. contributed to the initial steps of the project, M. M. supervised the whole project, analyzed the data, and wrote the paper.

Competing Interests Statement

The authors declare no competing interests.

Figures

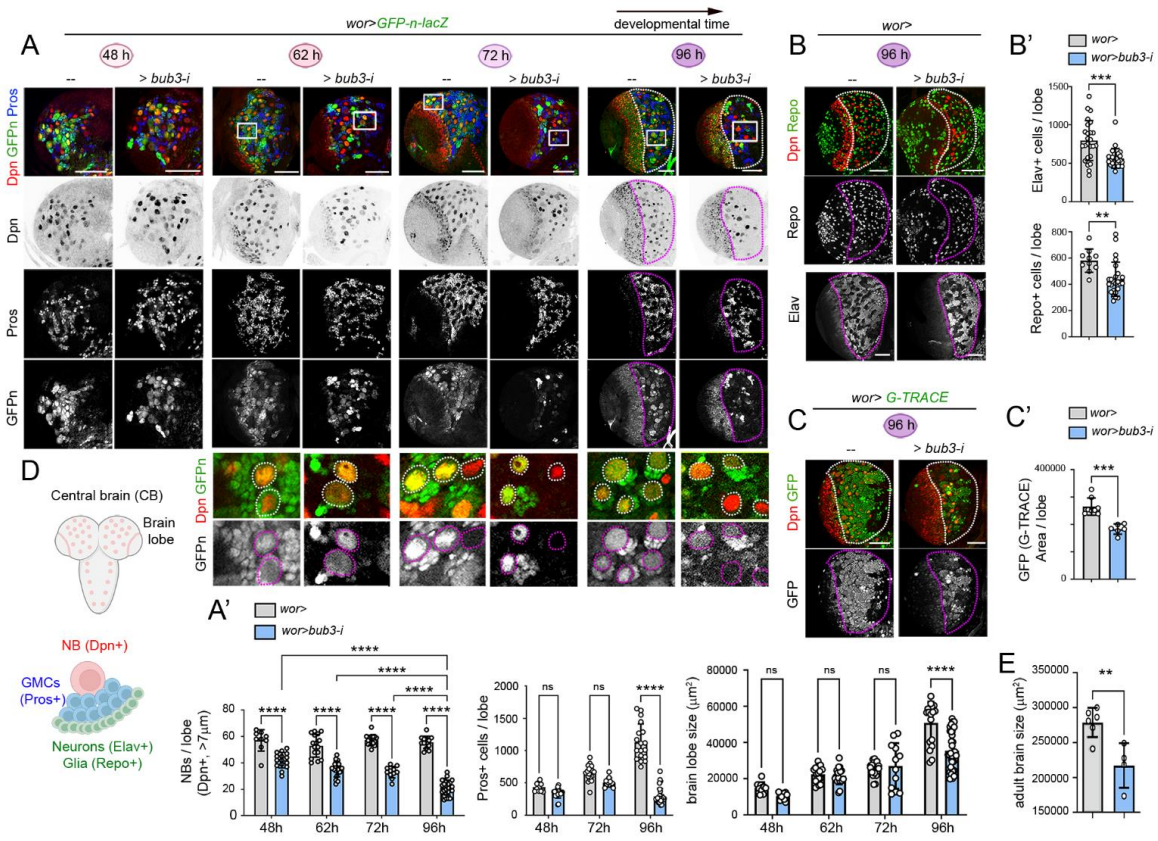

Fig. 1. Targeted depletion of SAC genes in neural stem cells induces microcephaly

(**A-C**) Larval brain lobes of larvae of different ages (in hours after egg laying, AEL) expressing an RNAi form for *bub3,* and a nuclear GFP/β-galactosidase fusion protein (**A**) or the G-TRACE cassette (**C**) under the control of the *worniu-gal4* driver, and stained for nuclear GFP (GFP, green and white, **A**, **C**), Dpn (red and black, **A**-**C**), Pros (blue and white, **A**), Repo (green and white, **B**), and Elav (white, **B**). High magnifications of the squared regions are shown in lower panels in **A**, where neuroblasts (NBs) are labeled by a white line. The central brain region is marked by a dashed line in 96 h AEL brains.

Scale bars, 50 µm. (**D**) Drawing of a larval brain and the NB lineage. Created in BioRender. Muzzopappa, M. (2026) https://BioRender.com/4fs9zf . (**A'**-**C'**, **E**) Histograms plotting the number of NBs (**A'**), the number of cells stained for Pros (**A'**), Repo and Elav (**B'**), and GFP (G-TRACE, **C'**) per brain lobe, and the size of the brain lobe of larvae (**A'**) or whole brain of adults (**E**) expressing the indicated transgenes and monitored at the indicated ages (**A'**-**C'**) or after adult hatching (**E**). Mean and standard deviation (SD) are shown. Two-way ANOVA (Šídák's multiple comparisons test for NBS/lobe and Pros+ cells/lobe, and Tukey's multiple comparisons test for brain lobe size) (**A'**), or Student's t-test (**B', C'**, **E**) were performed: * p<0.05, ** p<0.01, *** p<0.001, ****p <0.0001, n.s., not significant. See also Supplementary Fig. 1. Source data and p values are provided as a Source Data file.

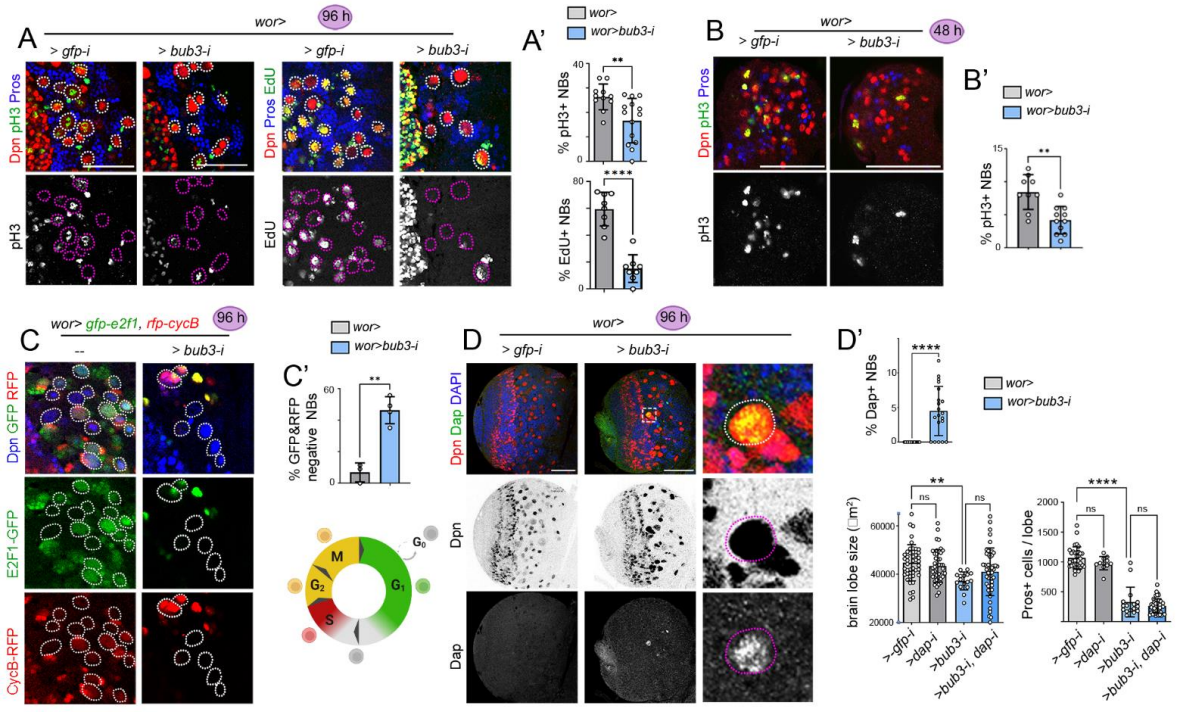

Fig. 2. Targeted depletion of SAC genes in neural stem cells induces a cell cycle arrest

(**A-D**) Larval brain lobes exposed to chronic expression of an RNAi form for *gfp* (as controls) or *bub3* under the control of the *worniu-gal4* driver and monitored at 96 h (**A**, **C**, **D**) or 48 h after egg laying (AEL, **B**) to visualize the expression of Dpn (red in **A**, **B**, red or black in **D**, and blue in **C**), Pros (blue, **A**, **B**), pH3 (green and white, **A**, **B**), EdU (green and white, **A**), FlyFucci (GFP-E2F1 in green, RFP-CycB in red, **C**), and Dap (green or white, **D**). **A** and **C** are high magnifications of central brain lobes

where neuroblasts (NBs) are marked by a dashed line. High magnification of the squared region in **D** is shown in the right panel. Scale bars, 50 µm. (**A'**, **B'**, **C'**, **D'**) Histograms plotting the percentage of NBs positive for pH3 or EdU (**A'**, **B'**), negative for GFP-E2F1 and RFP-CycB (**C'**), or positive for Dap (**D'**), and brain lobe size and number of GMCs per lobe (**D'**). Cartoon in **C'** was created in BioRender. Muzzopappa, M. (2026) https://BioRender.com/07s40bu. Mean and standard deviation (SD) are shown. Student's t-test (**A', B', C'**), Mann-Whitney test (for % Dap+ NBs) (**D'**), one-way ANOVA (for brain lobe size and Pros+ cells/lobe, Tukey's multiple comparisons test) (**D'**) were performed: * $p<0.05$, ** $p<0.01$, *** $p<0.001$, ****$p<0.0001$, n.s., not significant. Source data and p values are provided as a Source Data file.

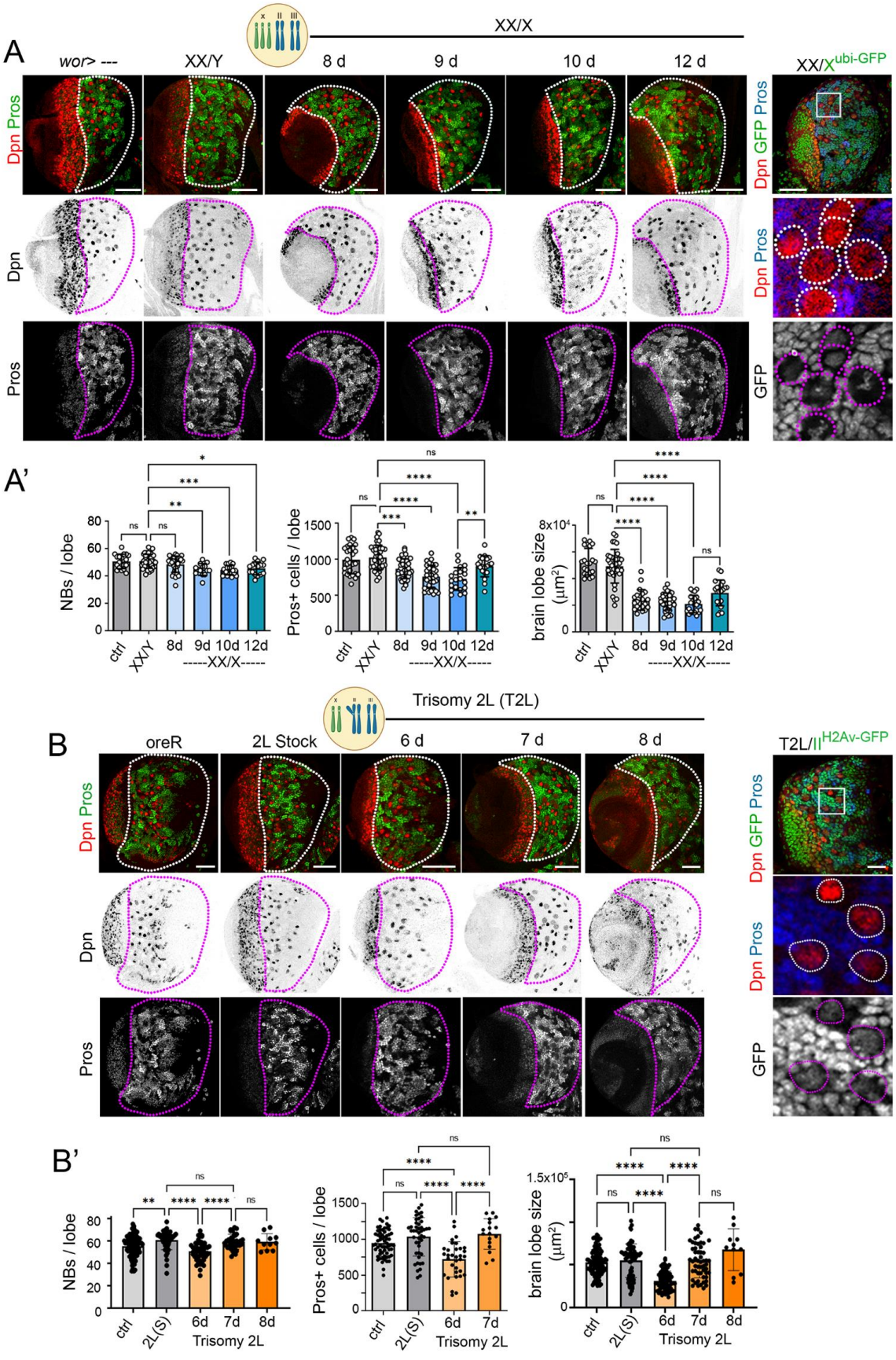
A
wor> ---
XX/Y
XX/X
8 d
9 d
10 d
12 d
XX/Xubi-GFP
Dpn Pros
Dpn GFP Pros
Dpn
Pros
GFP
A'
NBs / lobe
Pros+ cells / lobe
brain lobe size (µm²)
ctrl
XX/Y
8d
9d
10d
12d
-----XX/X-----
B
oreR
2L Stock
Trisomy 2L (T2L)
6 d
7 d
8 d
T2L/IIH2Av-GFP
B'
2L(S)
6d
7d
8d
Trisomy 2L

Fig. 3. Effects of trisomies on brain development

(**A**, **B**) Larval brain lobes of larvae trisomic for the X (**A**) or 2L (**B**) chromosomes and labeled to visualize the expression of Dpn (red or black), Pros (green, blue or white) and GFP (*ubi-GFP* transgene is located on the X, **A**, or second, **B**, chromosomes). Two controls were used: *wild-type* larvae, and larvae bearing compound chromosomes but maintaining euploidy. The central brain region is marked by a dashed line, and neuroblasts (NBs) are marked by a dashed line in the high magnification of the squared regions. Scale bars, 50 µm. Cartoons were created in BioRender. Muzzopappa, M. (2026) https://BioRender.com/t6of0bo (**A**) and Muzzopappa, M. (2026) https://BioRender.com/zxvjt79 (**B**)**.** (**A'**, **B'**) Histograms plotting the number of neuroblasts (NBs) and Pros-positive cells per lobe, and the size of the brain lobe of larvae of the indicated genotypes and monitored at the indicated ages (in days after egg laying, AEL). Mean and standard deviation (SD) are shown. One-way ANOVA (**A'**, **B'**, Tukey's multiple comparisons test) was performed: * $p<0.05$, ** $p<0.01$, *** $p<0.001$, **** $p<0.0001$, n.s., not significant. See also Supplementary Fig. 2. Source data and p values are provided as a Source Data file.

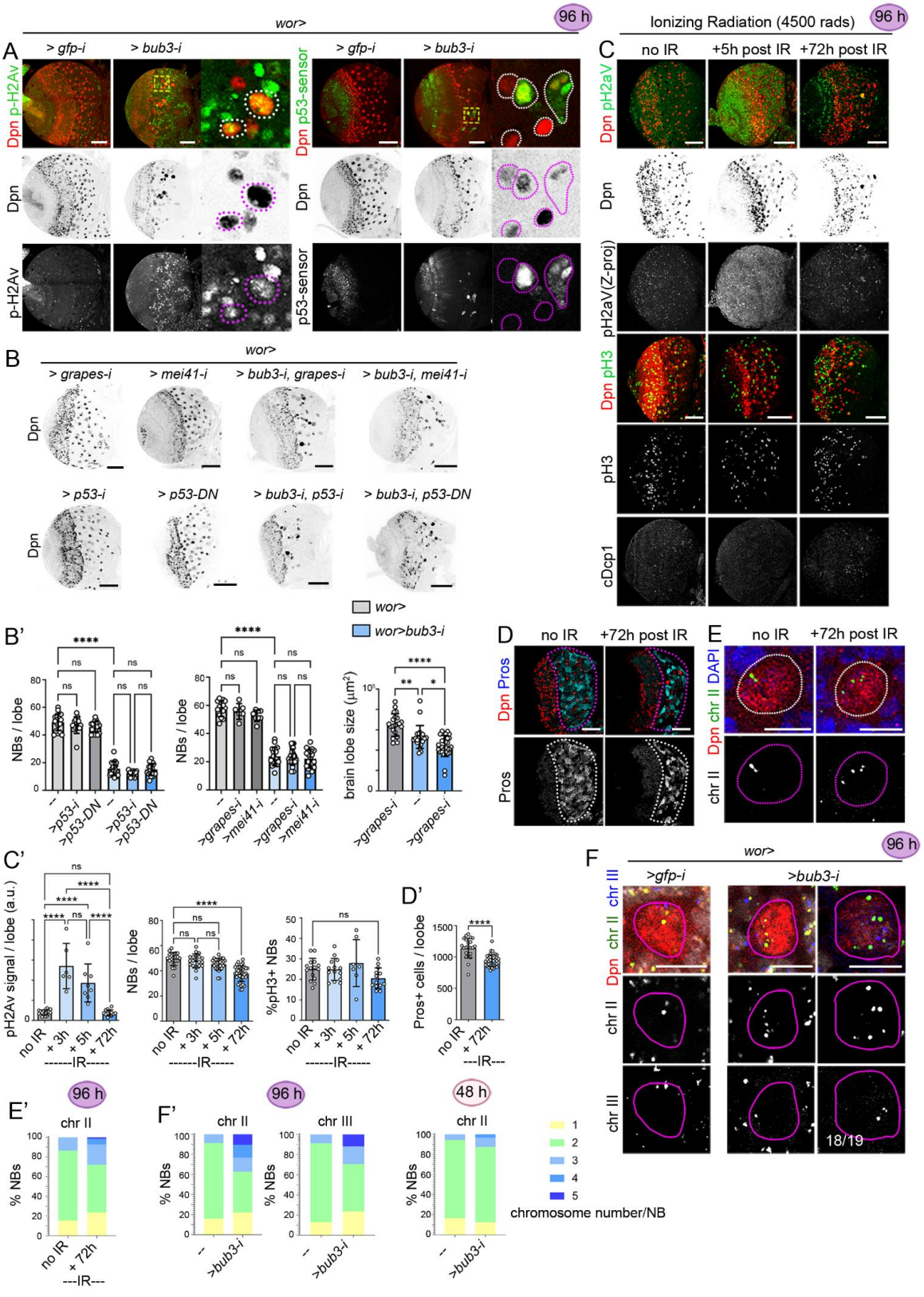

771

772 **Fig. 4. A discrete role of DNA damage on neural stem cell viability**

(**A**-**F**) Larval brain lobes and NBs expressing the indicated transgenes under the control of the *worniu-gal4* driver (**A**, **B**, **F**) or subjected to ionizing radiation 5 or 72 h before dissection (**C**-**E**) and labeled to visualize the expression of Dpn (red or black, **A**-**F**), pH2Av (green or white, **A**, **C**), p53 sensor (green or white, **A**), pH3 (green or white, **C**), cDcp1 (white, **C**), Pros (blue or white, **D**), chromosome II (green and white, **E**, **F**), and chromosome III (blue and white, **F**). Neuroblasts (NBs) are marked by a dashed line in the high magnification of the squared regions in **A** and in **E**, and in **F**. Central brain is marked by a dashed line in **D**. The ratio of NBs with an unbalanced number of chromosomes is shown in **F**. Scale bars, 50 µm. (**B'**-**F'**) Histograms plotting the number of NBs (**B'**, **C'**), Pros-positive cells (**D'**) and pH2Av signal (**C'**) per brain lobe, brain lobe size (**B'**), and percentage of pH3-positive NBs (**C'**) or NBs containing different numbers of chromosome II and III (**E'**, **F'**) of larvae subjected to transgene expression or ionizing radiation. n(NBs) in E'= 68 (control) and 52 (IR); n(NBs) in F'= 81 (control, chr II, 96h after egg laying, AEL), 86 (bub3-RNAi, chr II, 96h AEL), 23 (control, chr III, 96h AEL), 17(bub3-RNAi, chr III, 96 h AEL), 18 (control, chr II, 48h AEL) and 32 (bub3-RNAi, chr II, 48h AEL). Mean and standard deviation (SD) are shown. One-way ANOVA (**B', C'**, Tukey's multiple comparisons test), Student's t-test (**D'**), and two-way ANOVA (**E'**, **F'**, Šídák's multiple comparisons test) were performed: * $p<0.05$, ** $p<0.01$, *** $p<0.001$, **** $p<0.0001$, n.s., not significant. See also Supplementary Fig. 3. Source data and p values are provided as a Source Data file.

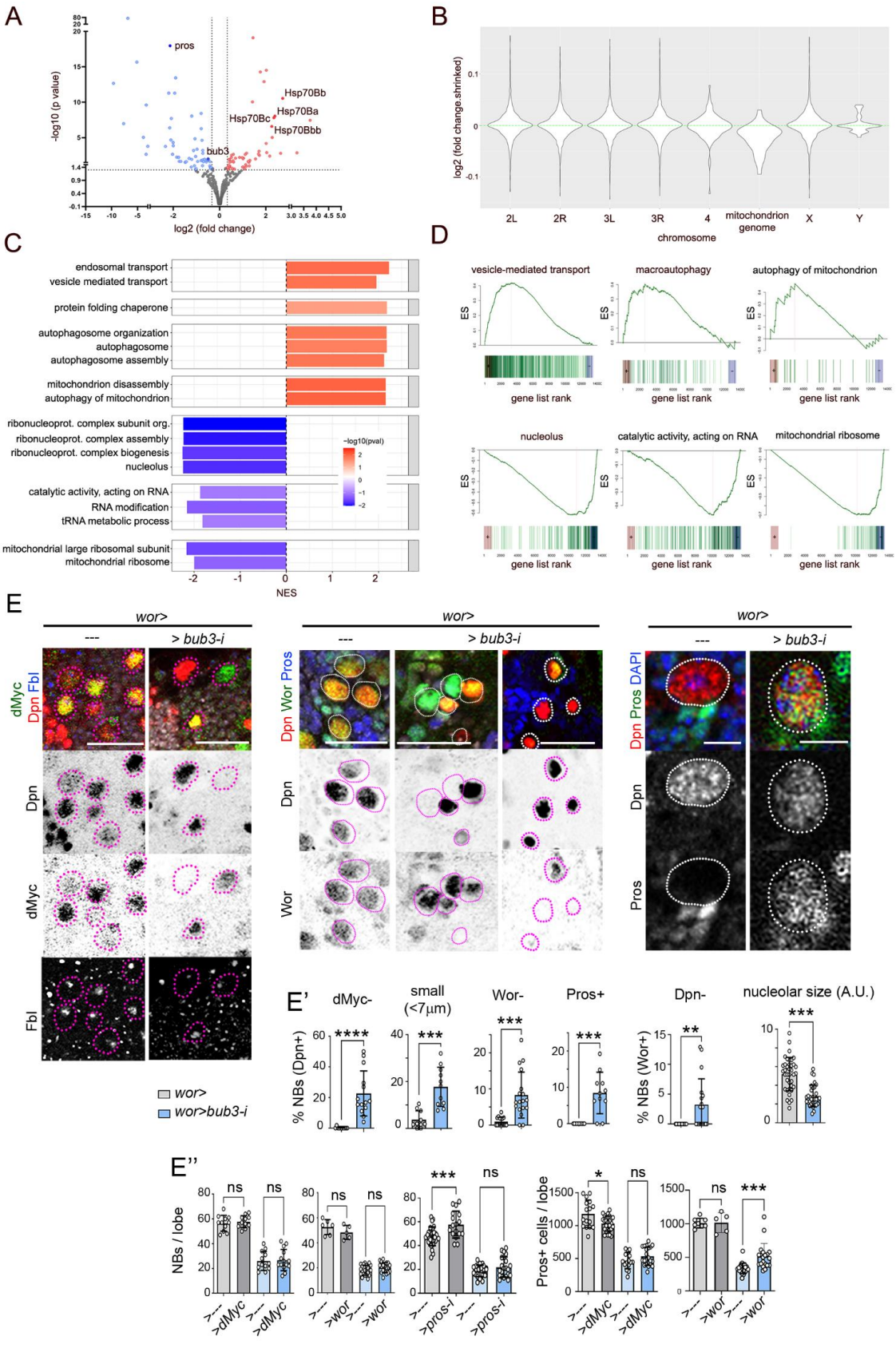
A
pros
Hsp70Bb
Hsp70Ba
Hsp70Bc
Hsp70Bbb
bub3
-log10 (p value)
log2 (fold change)
B
log2 (fold change.shrinked)
2L
2R
3L
3R
4
mitochondrion genome
X
Y
chromosome
C
endosomal transport
vesicle mediated transport
protein folding chaperone
autophagosome organization
autophagosome
autophagosome assembly
mitochondrion disassembly
autophagy of mitochondrion
ribonucleoprot. complex subunit org.
ribonucleoprot. complex assembly
ribonucleoprot. complex biogenesis
nucleolus
catalytic activity, acting on RNA
RNA modification
tRNA metabolic process
mitochondrial large ribosomal subunit
mitochondrial ribosome
-log10(pval)
NES
D
vesicle-mediated transport
macroautophagy
autophagy of mitochondrion
nucleolus
catalytic activity, acting on RNA
mitochondrial ribosome
ES
gene list rank
E
wor>

> bub3-i
dMyc Dpn Fbl
Dpn
dMyc
Fbl
Dpn Wor Pros
Wor
Dpn Pros DAPI
Pros
wor>
wor>bub3-i
E'
dMyc-
small (<7μm)
Wor-
Pros+
Dpn-
nucleolar size (A.U.)
% NBs (Dpn+)
% NBs (Wor+)
E''
NBs / lobe
Pros+ cells / lobe
>dMyc
>wor
>pros-i

790

Fig. 5. Complex aneuploidies induce loss of stemness

(**A**-**D**) Transcriptional changes of larval brain lobes exposed to chronic expression of an RNAi form of *bub3* (SAC depletion) when compared to controls (expressing *gfp-RNAi*) under the control of the *worniu-gal4* driver and monitored at 96 h after egg laying (AEL). In the volcano plot (**A**), significantly up- (red) or down-regulated (blue) genes ($p < 0.05$, abs (fold change) ≥ 1.25) are highlighted. Relevant genes are labeled with their corresponding symbols. Fold changes and p-values were calculated using the DESeq2 R package. p-values were adjusted for multiple comparisons with the Benjamini-Hochberg algorithm. Violin plot in (**B**) represents the fold change of those genes located in each of the chromosomes and the mitochondrial genome. Bar plot in (**C**) represents GO and KEGG pathway enrichment analysis for up- (red) and down-regulated (blue) gene sets. Statistics from the roastgsa enrichment algorithm of selected pathways are shown. P-value sign corresponds to that of the normalized enrichment score (NES). See the methods section for details on methodology. Gene set enrichment analysis of some GO and KEGG pathways are shown in **D**. (**E**) High magnifications of larval brain lobes expressing the indicated transgenes under the control of the *worniu-gal4* driver and labeled to visualize the expression of Deadpan (Dpn, red or black), dMyc (green or black), and Fibrilarin (Fbl, blue or white). Neuroblasts (NBs) are marked by a dashed line. Scale bars, 25 µm (1st and 2nd panel) and 7 µm (3rd panel). **(E')** Histograms plotting the percentage of NBs losing dMyc expression, percentage of cells <7 µm Dpn+, percentage of NBs losing Wor expression, percentage of NBs losing Dpn expression, percentage of NBs (Dpn+, >7 µm) with Pros expression, and size of nucleolus according to Fbl signal. The number of NBs and Prospero-positive cells per brain lobe (**E''**) of larvae subjected to the expression of the indicated transgenes. Mean and standard deviation (SD) are shown. Mann-Whitney test (**E'**, dMyc-, Dpn-, Pros+), Student's t-test (**E'**, small, Wor-, nucleolar size), and one-way ANOVA (**E'',** Tukey's multiple comparisons test) were performed:* $p<0.05$, ** $p<0.01$, *** $p<0.001$, **** $p<0.0001$, n.s., not significant. See also Supplementary Fig. 4, Supplementary Fig. 5 and Supplementary Data 1. Source data and p values are provided as a Source Data file.

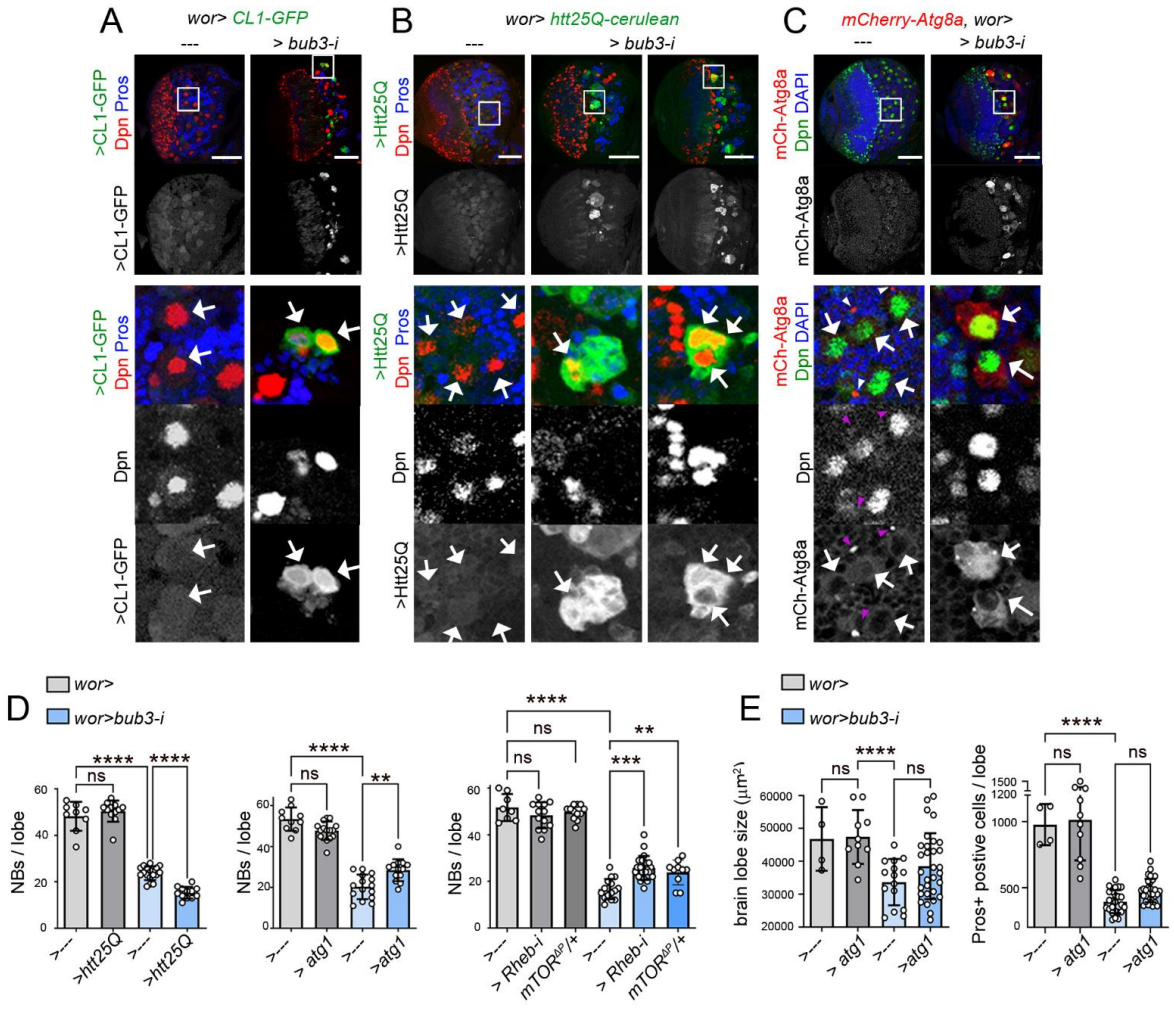

Fig. 6. Proteostasis failure contributes to the loss of neural stem cells carrying complex aneuploidies

(**A**-**C**) Larval brain lobes expressing the indicated transgenes under the control of the *worniu-gal4* driver and labeled to visualize the expression of Dpn (red, green or white), Pros (blue, **A**, **B**), DAPI (blue, **C**), CL1-GFP (green or white, **A**), Htt25Q (green or white, **B**), and mCh-Atg8A (red or white, **C**). High magnifications of the squared regions are shown in the lower panels where neuroblasts (NBs) are marked by an arrow. Small arrowheads in C point to mCh-Atg8A-postive dots in progeny cells of wild type brains. Scale bars, 50 µm. (**D, E**) Histograms plotting the number of NBs (**D**) and Prospero-positive cells (**E**) per brain lobe, and brain lobe size (**E**) of larvae subjected to the expression of the indicated transgenes or heterozygous for *mTOR*. Mean and standard deviation (SD) are shown. One-way ANOVA (**D**, **E**, Tukey's multiple comparisons test) was performed:* p<0.05, ** p<0.01, *** p<0.001, ****

p<0.0001 n.s., not significant. See also Supplementary Fig. 6. Source data and p values are provided as a Source Data file.

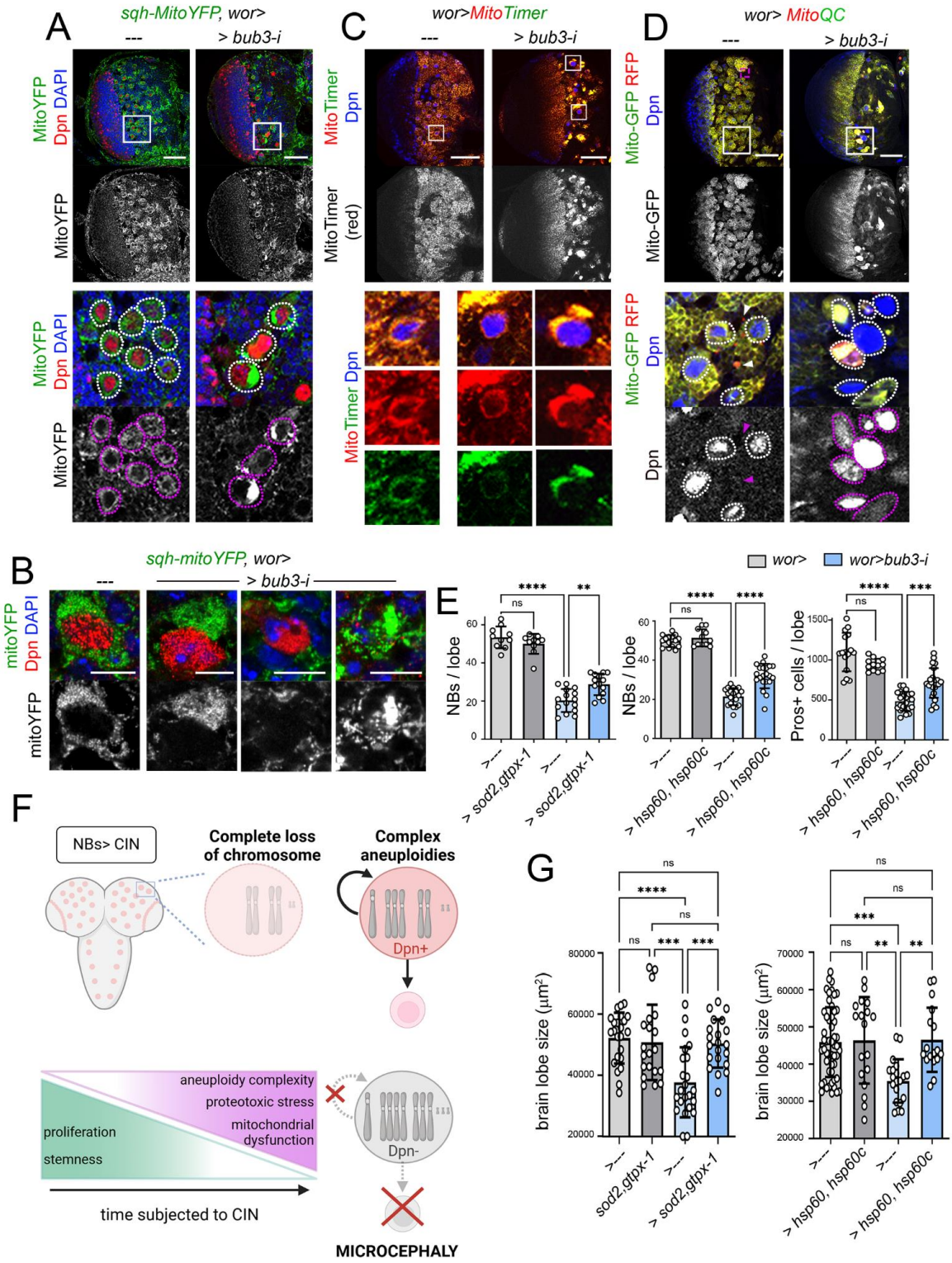

Fig. 7. Mitochondrial dysfunction contributes to the loss of neural stem cells carrying complex aneuploidies

(**A**-**D**) Larval brain lobes and neuroblasts (NBs) expressing the indicated transgenes under the control of the *worniu-gal4* driver and labeled to visualize the expression of Dpn (red, blue and white), sqh-Mito-YFP (green or white, **A**, **B**), Mito-Timer (green or white, **C**), and Mito-QC (green, red and white, **D**). In **A**, **C**, and **D**, high magnifications of the squared regions are shown in the lower panels and NBs are marked by a dashed line. Scale bars, 50 µm (A, C, D) and 7 µm (B). (**E, G**) Histograms plotting the number of NBs or Prospero-positive cells per brain lobe (**E**) and the brain lobe size (G) of larvae subjected to the expression of the indicated transgenes. Mean and standard deviation (SD) are shown. One-way ANOVA (**E**, **G** Tukey's multiple comparisons test) was performed: * $p<0.05$, ** $p<0.01$, *** $p<0.001$, **** $p<0.0001$, n.s., not significant. (**F**) Cartoon summarizing the major cellular mechanisms underlying CIN induced microcephaly. Upon CIN induction in NBs, the accumulation of an unbalanced number of chromosomes consisting of multiple gains and/or losses leads to stemness loss (loss of NB identity and proliferative capacity) as a result of proteotoxic stress and mitochondria dysfunction. The complete loss of chromosomes is known to be cell lethal. Created in BioRender. Muzzopappa, M. (2026) https://BioRender.com/szbcyiw. See also Supplementary Fig. 7. Source data and p values are provided as a Source Data file.

Supplementary Information

Proteostasis failure and mitochondrial dysfunction contribute to chromosomal instability-induced microcephaly

Amanda González-Blanco, Adrián Acuña-Higaki, David Boettger, Jery Joy, and Marco Milán *

Supplementary Figures:

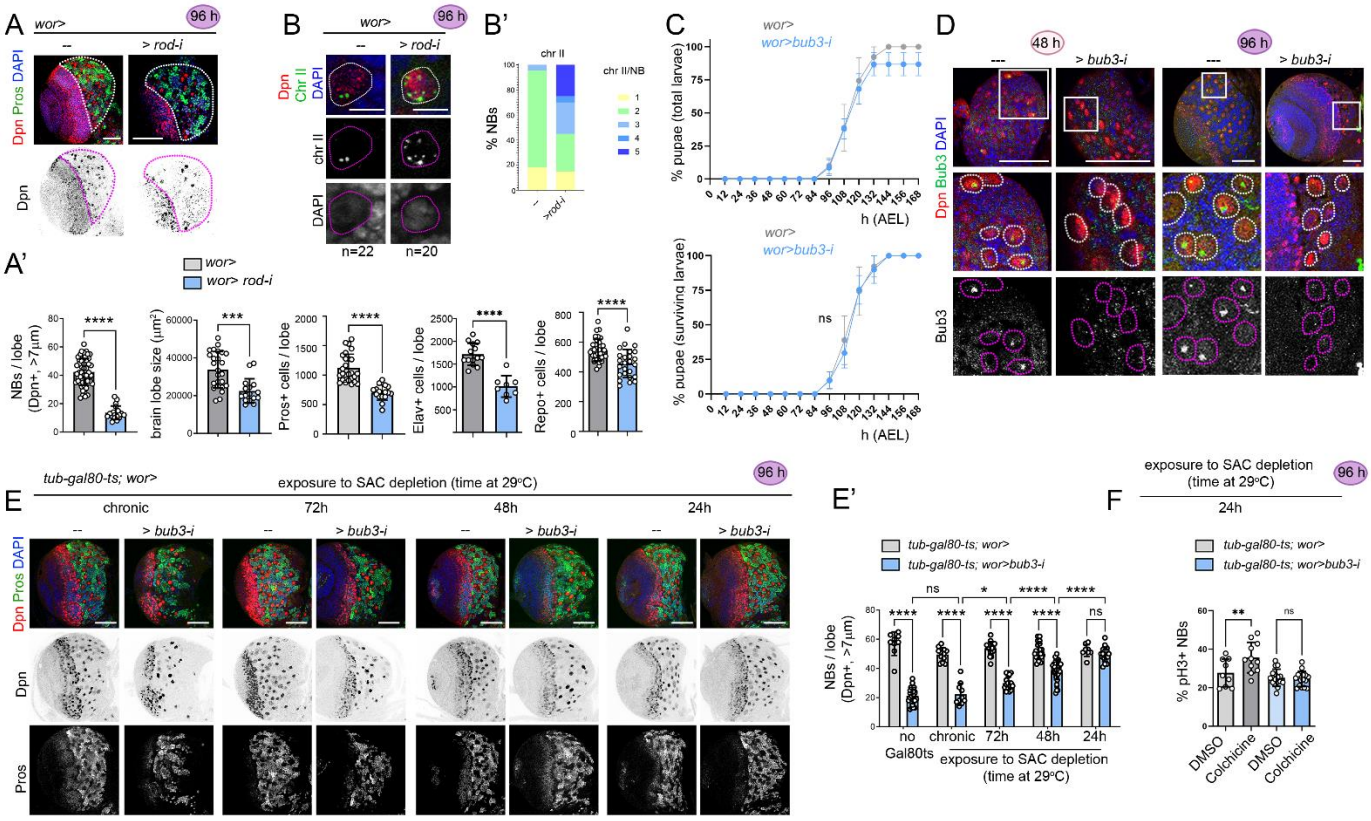

Supplementary Fig. 1. Delayed response of neural stem cells to SAC depletion (related to Fig. 1)

(**A**, **B**, **D, E**) Larval brain lobes (**A**, **D, E**) or neuroblasts (**B**) exposed to the expression of an RNAi form for *rod* (**A**, **B**) or *bub3* (**D**, **E**) under the control of the *worniu-gal4* driver, either chronically (since the embryo, **A**, **B**, **D**, and first panels in **E**), or during the indicated periods (in hours in **E**) and monitored at 48h (**D**) or 96 h AEL (**A**, **B**, **E**) to visualize the expression of Dpn (red and black), Pros (green and white, **A**, **E**), Bub3 (green, **D**), DAPI (blue), and the number of chromosome II (green) in **B**. Scale bars, 50 µm (**A**, **D**, **E**) and 7 µm (**B**). (**A'**, **B'**, **E'**) Histograms plotting the number of neuroblasts (NBs, **A'**, **E'**), Pros-positive, Repo-positive and Elav-positive (**A'**) per brain lobe, the size of the brain lobe (**A'**) and the percentage of NBs containing different numbers chromosome II (**B'**) of larvae expressing the indicated transgenes and exposed to SAC depletion during the indicated periods (in hours). 22 control NBs and 20 *rod*-depleted NBs were quantified in **B'**. (**C**) Developmental timing of larvae expressing the indicated transgenes under the control of the *worniu-gal4* driver chronically (since the embryo), where either all larvae (top graph) or only

the surviving pupae (bottom graph) were taken into consideration. (**F**) Histogram plotting the percentage of NBs in mitosis of larvae expressing the indicated transgenes, exposed to SAC depletion for 24 h and cultured in DMSO or colchicine treatment for 4 h. Mean and standard deviation (SD) are shown. Student's t-test (**A'**) or two-way ANOVA (Šídák's multiple comparisons test, **C** and **E'**) were performed: * p<0.05, ** p<0.01, *** p<0.001, ****p <0.0001, n.s., not significant. Source data (including p values and number of samples) are provided as a Source Data file.

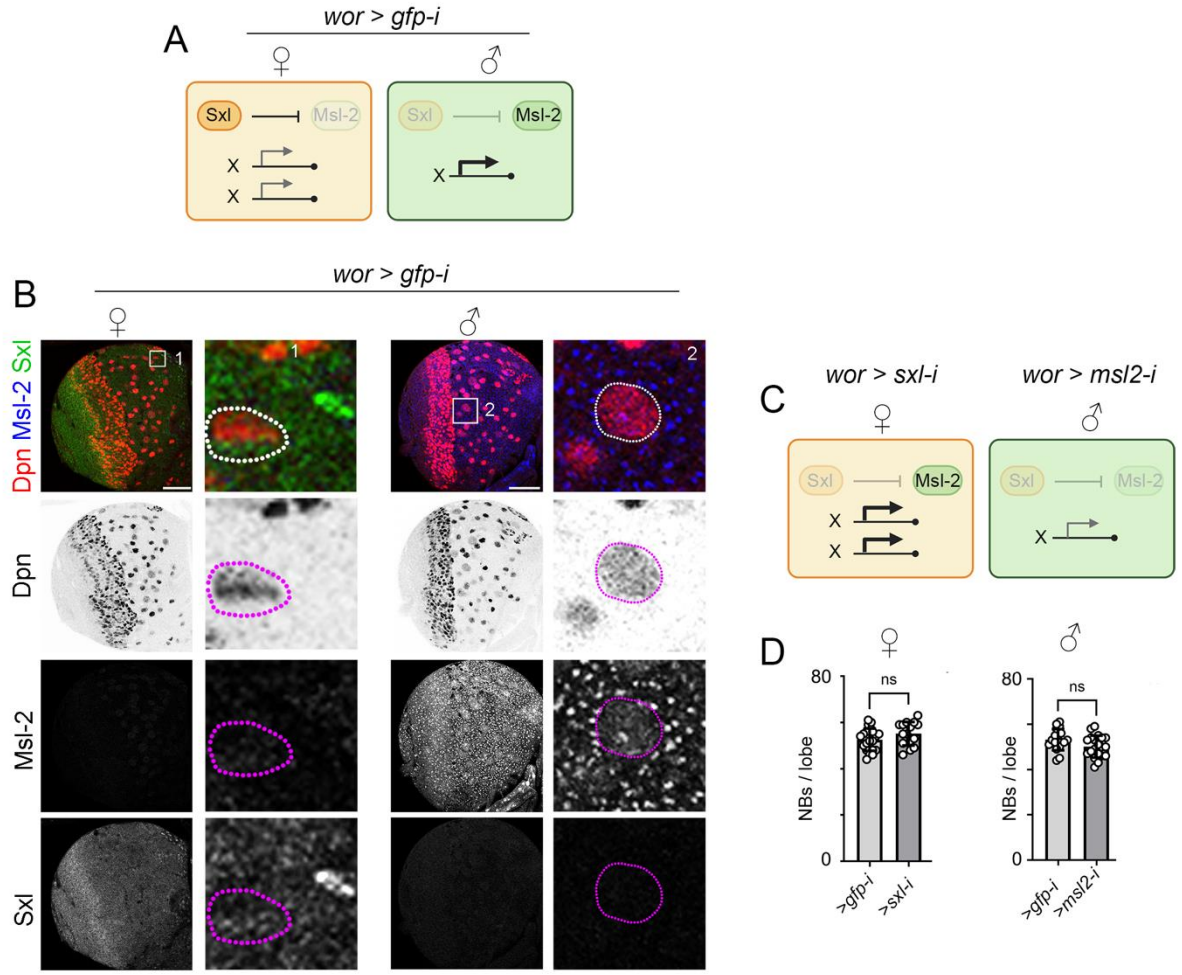

Supplementary Fig. 2. Effects of gene dosage imbalance on neural stem cell viability (related to Fig. 3)

(**A**, **C**) Cartoons depicting the expected expression levels of X-linked genes according to the presence of Sxl or Msl2 in the indicated sexes and genotypes. Created in BioRender. Muzzopappa, M. (2026) https://BioRender.com/qod1bd0 (**A**) and Muzzopappa, M. (2026) https://BioRender.com/sk0rcq3 (**C**). (**B**)

Larval brain lobes of female and male larvae expressing the indicated transgene under the control of the *worniu-gal4* driver and labeled to visualize the expression of Dpn (red or black), Msl-2 (blue or white) and Sxl (green or white). Neuroblasts (NBs) are marked by a dashed line in the high magnification of the squared regions. Scale bars, 50 µm. (**D**) Histograms plotting the number of NBs per brain lobe of female and male larvae expressing the indicated genotypes under the control of the *worniu-gal4* driver. Mean and standard deviation (SD) are shown. Student's t-test (**D**) was performed: * p<0.05, ** p<0.01, *** p<0.001, ****p <0.0001, n.s., not significant. Source data (including p values and number of samples) are provided as a Source Data file.

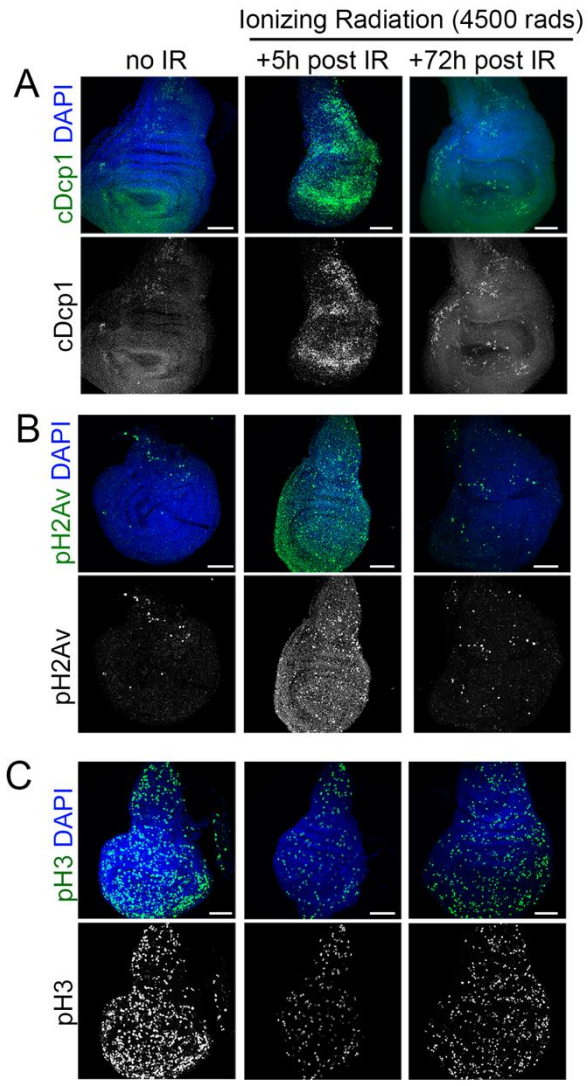

Supplementary Fig. 3. Effects of Ionizing Radiation on larval epithelial cells (related to Fig. 4)

(**A**-**C**) Late third instar wing discs subjected to ionizing radiation 5 and 72 h before dissection and labeled to visualize DAPI (blue), cDcp1 (green and white, **A**), pH2Av (green and white, **B**), and pH3 (green and white, **C**). Untreated wing discs are shown in the first column. Scale bars, 50 µm.

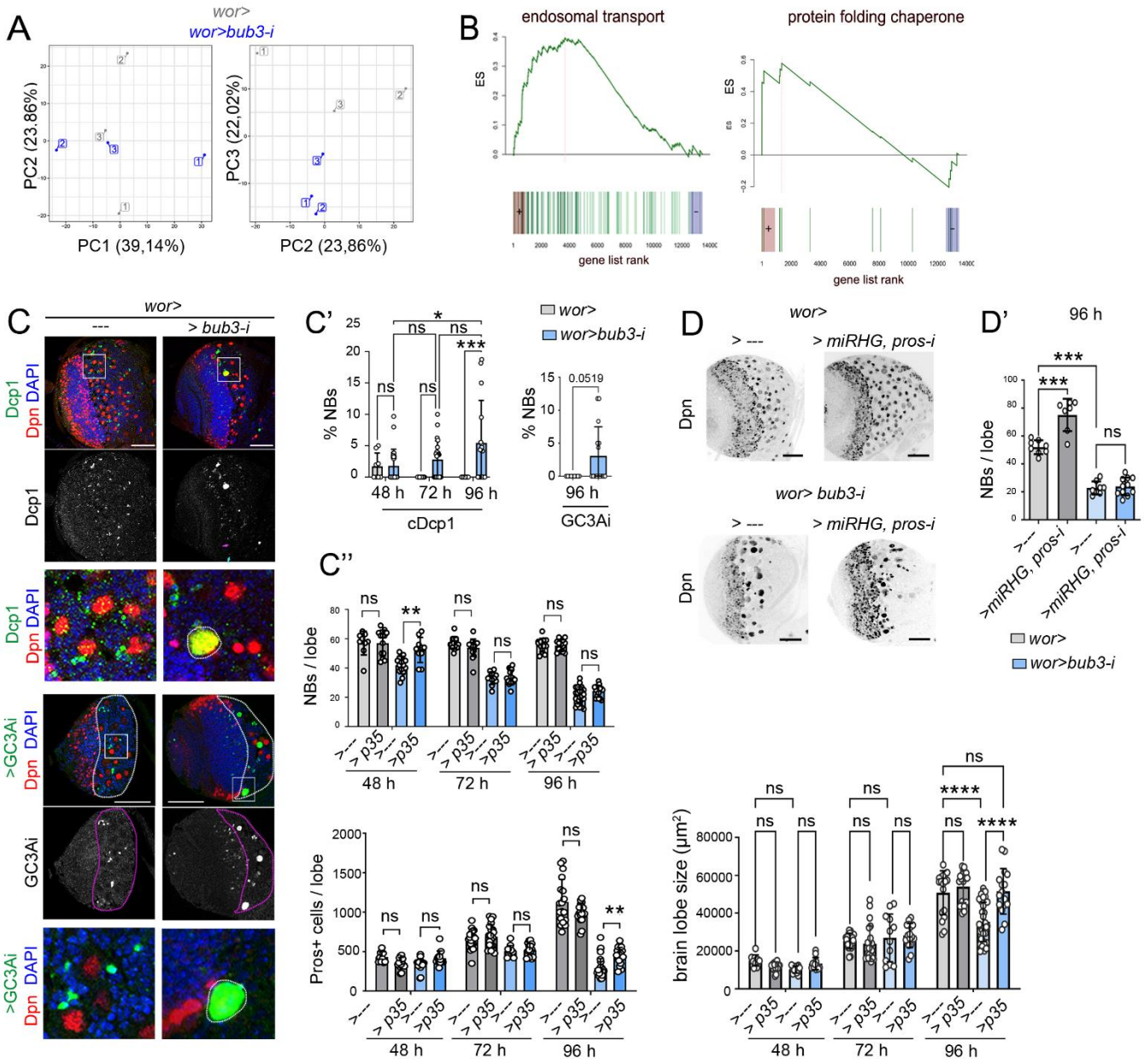

Supplementary Fig. 4. Apoptosis-independent elimination of neural stem cells carrying complex aneuploidies (related to Fig. 5)

(**A, B**) Transcriptional changes of larval brain lobes exposed to chronic expression of an RNAi form of *bub3* (SAC depletion) when compared to controls (expressing *gfp-RNAi*) under the control of the *worniu-gal4* driver and monitored at 96 h AEL. In (**A**), Principal Components (PC) of the normalized expression matrix 1, 2 and 3 are shown. In (**B**), mountain plots of gene set enrichment analysis of significantly up- or down-regulated GO and KEGG pathways are shown. (**C**) Larval brain lobes expressing the indicated transgenes under the control of the *worniu-gal4* driver and labeled to visualize the expression of Dpn (red or black), cDcp1 (green and white, **A**, top panels), GC3Ai (green and white, bottom panels), and DAPI (blue). In **C**, high magnifications of the squared regions are shown in the lower panels and neuroblasts (NBs) are marked by a dashed line. Scale bars, 50 µm. **(C'**, **C'')** Histograms plotting the percentage of NBs labeled with cDcp1 or GC3Ai (**C'**), the number of NBs and Prospero-positive cells per brain lobe and brain lobe size (**C''**) of larvae subjected to the expression of the indicated transgenes in time points. (D) Larval brain lobes expressing the indicated transgenes under the control of the *worniu-gal4* driver and labeled to visualize the expression of Dpn. (D') Histogram plotting the number of NBs per brain lobe of larvae subjected to the expression of the indicated transgenes at 96 h AEL. Mean and standard deviation (SD) are shown. Mann Whitney test (C'), two-way ANOVA (C'', Tukey's multiple comparisons test), and one-way ANOVA (D', Tukey's multiple comparisons test) were performed: * $p<0.05$, ** $p<0.01$, *** $p<0.001$, **** $p< 0.0001$, n.s., not significant. Source data (including p values and number of samples) are provided as a Source Data file.

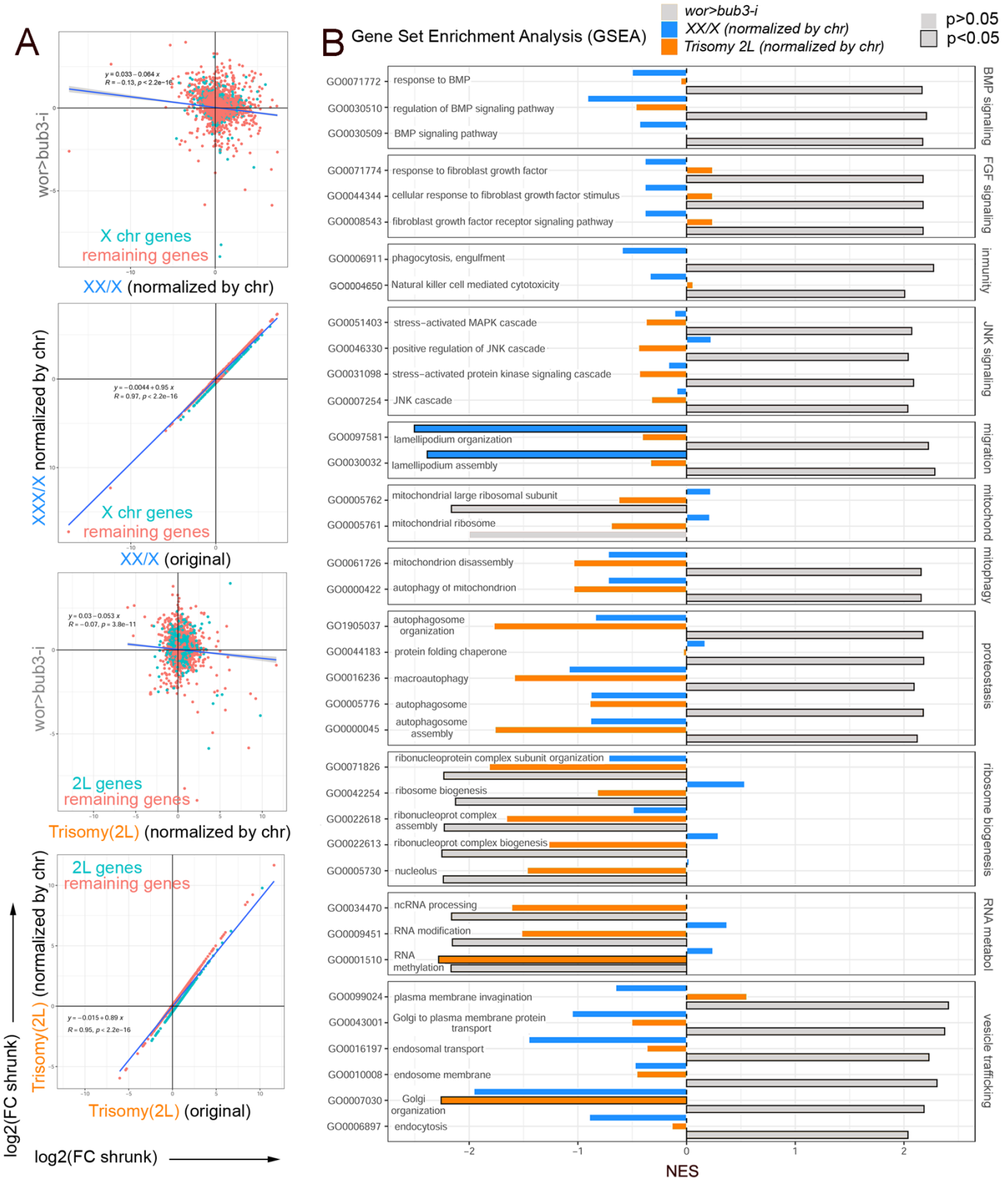

Supplementary Fig. 5. Different transcriptional response to complex and simple aneuploidies (related to Fig. 5)

(**A**) Plots representing the fold changes in larval brains of the indicated genotypes when compared to the corresponding experimental controls (see Materials and Methods for details). Fold-changes of trisomies before (original) and after normalization by chromosome are shown. The genes located in the trisomy and in the remaining chromosomes are labeled in blue and orange, respectively. (**B**) Bar plot representing NES and p-values of selected GO and KEGG pathways for up- (NES>0) and down-regulated (NES<0) gene sets in larval brains of the indicated genotypes when compared to the experimental controls. NES analysis of trisomy of the X (in blue) and 2L (in orange) was performed after normalization per chromosome (see Materials and Methods for details).

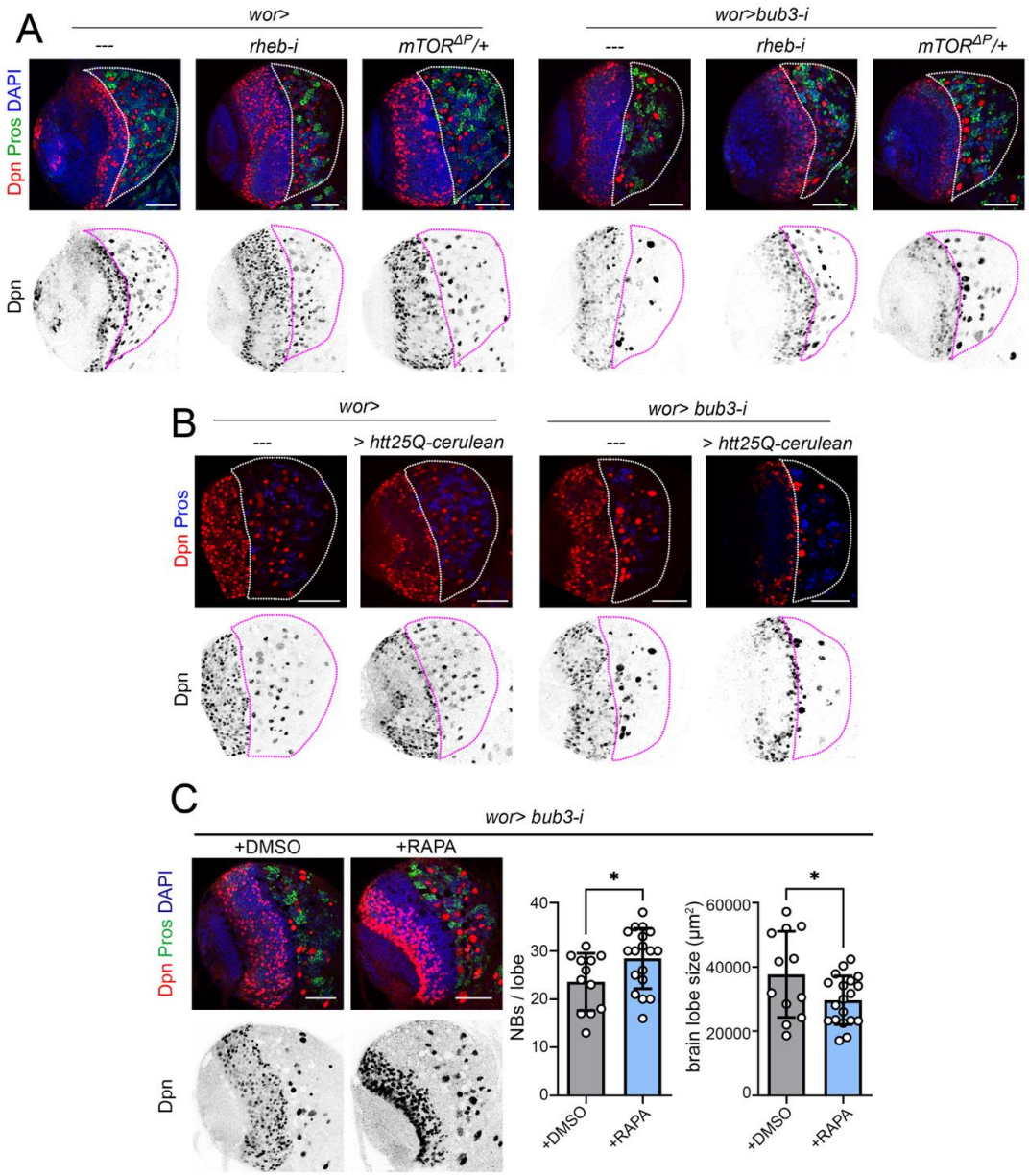

Supplementary Fig. 6. TOR depletion rescues the loss of neural stem cells carrying complex aneuploidies (related to Fig. 6)

(**A**-**C**) Larval brain lobes expressing the indicated transgenes under the control of the *worniu-gal4* driver and labeled to visualize the expression of Dpn (red and black), Pros (green), and DAPI (blue), and histograms (**C**) plotting number of neuroblasts (NBs) per brain lobe and brain lobe size of larvae subjected to the expression of the indicated transgenes. Mean and standard deviation (SD) are shown. Student t-test was performed: * $p<0.05$. Scale bars, 50 µm. In **C**, larvae were fed with Rapamycin (RAPA, see Materials and Methods). Source data (including p values and number of samples) are provided as a Source Data file.

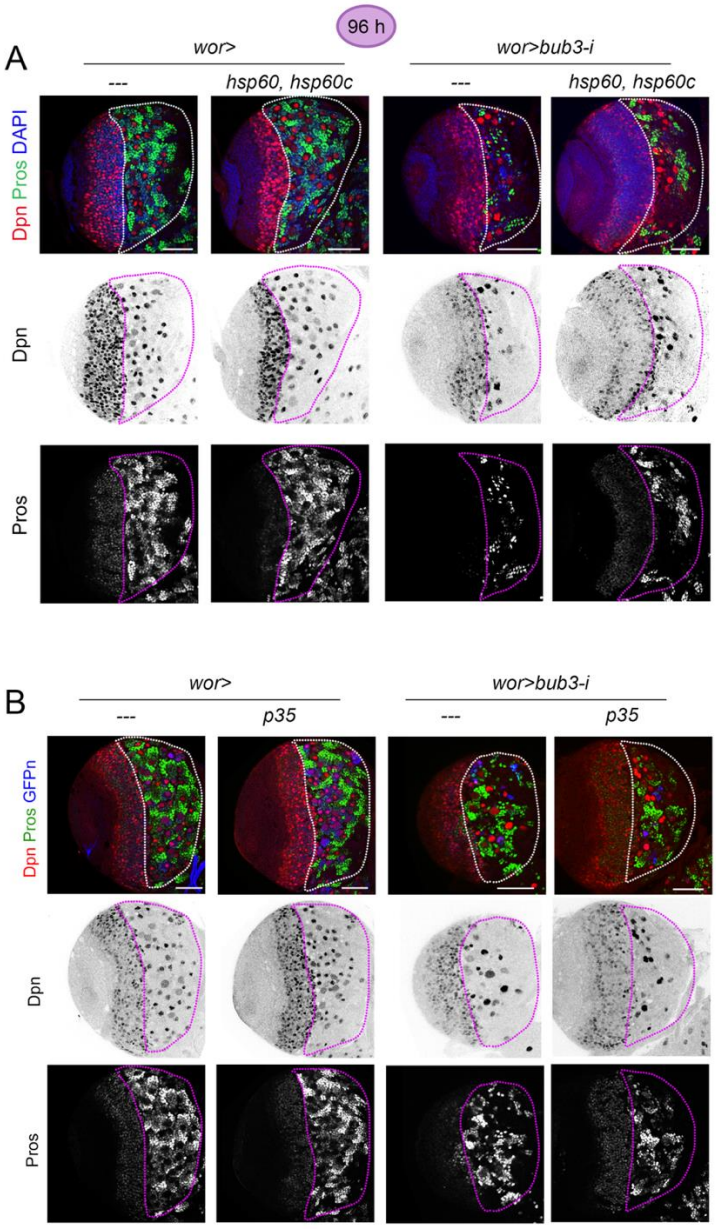

Supplementary Fig. 7. Different impact of mitochondrial chaperones and apoptosis blockade on the loss of neural stem cells carrying complex aneuploidies and brain size (related to Fig. 7)

(**A, B**) Larval brain lobes expressing the indicated transgenes under the control of the *worniu-gal4* driver and labeled to visualize the expression of Dpn (red and black), Pros (green and white), DAPI (blue, A) and GFPn (blue (B). Scale bars, 50 µm.